Eur. Phys. J. C (2015) 75:183
DOI 10.1140/epjc/s10052-015-3385-x

THE EUROPEAN PHYSICAL JOURNAL C

Regular Article - Theoretical Physics

New mechanism for Type-II seesaw dominance in SO(10) with low-mass Z', RH neutrinos, and verifiable LFV, LNV and proton decay

Bidyut Prava Nayak[a], **Mina Ketan Parida**[b]

Centre of Excellence in Theoretical and Mathematical Sciences, Siksha 'O' Anusandhan University, Khandagiri Square, Bhubaneswar 751030, Odisha, India

Received: 30 October 2014 / Accepted: 31 March 2015 / Published online: 1 May 2015

Abstract The dominance of Type-II seesaw mechanism for the neutrino masses has attracted considerable attention because of a number of advantages. We show a novel approach to achieve Type-II seesaw dominance in non-supersymmetric SO(10) grand unification where a low-mass Z' boson and specific patterns of right-handed neutrino masses are predicted within the accessible energy range of the Large Hadron Collider. In spite of the high value of the seesaw scale, $M_{\Delta_L} \simeq 10^8$–10^9 GeV, the model predicts new dominant contributions to neutrino-less double beta decay in the W_L–W_L channel close to the current experimental limits via exchanges of heavier singlet fermions used as essential ingredients of this model even when the light active neutrino masses are normally hierarchical or invertedly hierarchical. We obtain upper bounds on the lightest sterile neutrino mass $m_s \lesssim 3.0\,\text{GeV}$, 2.0 GeV and 0.7 GeV for normally hierarchical, invertedly hierarchical and quasi-degenerate patterns of light-neutrino masses, respectively. The underlying non-unitarity effects lead to lepton flavour violating decay branching ratios within the reach of ongoing or planned experiments and the leptonic CP-violation parameter nearly two order larger than the quark sector. Some of the predicted values on the proton lifetime for $p \to e^+\pi^0$ are found to be within the currently accessible search limits. Other aspects of model applications including leptogenesis etc. are briefly indicated.

1 Introduction

Experimental evidence on tiny neutrino masses and their large mixings has attracted considerable attention as regards physics beyond the standard model (SM) leading to different mechanisms for neutrino mass generation. Most of these models are based upon the underlying assumption that neutrinos are Majorana fermions that may manifest in the detection of events in neutrino-less double beta ($0\nu\beta\beta$) decay experiments on which a number of investigations are in progress [1–9]. Theories of neutrino masses and mixings are placed on a much stronger footing if they originate from left–right symmetric (LRS) [10–13] grand unified theories such as SO(10) where, besides grand unification of three forces of nature, P (for parity) and CP-violations have spontaneous-breaking origins, the fermion masses of all the three generations are adequately fitted [14], all the 15 fermions plus the right-handed neutrino (N) are unified into a single spinorial representation **16** and the canonical (≡Type-I) seesaw formula for neutrino masses is predicted by the theory. More recently a non-SUSY SO(10) origin of cold dark matter has also been suggested [15–19]. Although a Type-I seesaw formula was also proposed by using extensions of the SM [20–27], it is well known that this was advanced even much before the atmospheric neutrino oscillation data [28] and it is interesting to note that Gell-Mann, Ramond and Slansky had used the left–right symmetric SO(10) theory and its Higgs representations 10_H, 126_H to derive it. A special feature of left–right (LR) gauge theories and SO(10) grand unification is that the canonical seesaw formula for the neutrino masses is always accompanied by a Type-II seesaw formula [29–31] for the Majorana neutrino mass matrix,

$$\mathcal{M}_\nu = m_\nu^{II} + m_\nu^{I}, \tag{1}$$

$$m_\nu^{I} = -M_D \frac{1}{M_N} M_D^T, \tag{2}$$

$$m_\nu^{II} = f v_L \tag{3}$$

where $M_D(M_N)$ is the Dirac (RH-Majorana) neutrino mass, v_L is the induced vacuum expectation value (VEV) of the left-handed (LH) triplet Δ_L, and f is the Yukawa coupling of the triplet. Normally, because of the underlying quark–lepton

[a] e-mail: bidyutprava25@gmail.com
[b] e-mail: minaparida@soauniversity.ac.in

symmetry in SO(10), M_D is of the same order as M_u, the up-quark mass matrix. Then the neutrino oscillation data forces the canonical seesaw scale to be large, $M_N \geq 10^{11}$ GeV. Similarly the Type-II seesaw scale is also large. With such high seesaw scales, these two mechanisms in SO(10) cannot be directly verified at low energies or by the Large Hadron Collider (LHC) except for the indirect signature through the light active neutrino mediated $0\nu\beta\beta$ decay and, possibly, leptogenesis.

It is well known that the theoretical predictions of branching ratios for LFV decays such as $\mu \to e\gamma$, $\tau \to \mu\gamma$, $\tau \to e\gamma$ and $\mu \to e\bar{e}e$ closer to their experimental limits are generic features of SUSY GUTs even with high seesaw scales but, in non-SUSY models with such seesaw scales, they are far below the experimental limits. Recently they have been also predicted to be experimentally accessible along with low-mass W_R, Z_R bosons through TeV scale gauged inverse seesaw mechanism [32] in SUSY SO(10). In the absence of any evidence of supersymmetry so far, alternative non-SUSY SO(10) models have been found with predictions of substantial LFV decays and TeV scale Z' bosons. Although two-step breakings of LR gauge theory was embedded earlier in non-SUSY GUTs with low-mass Z' (For earlier work on, Z' boson in GUTs embedding two-step breaking of left-right gauge symmetry, see [33–35]), its successful compliance with neutrino oscillation data has been possible in the context of inverse seesaw mechanism and predictions of LFV decays [36], or with the predictions of low-mass W_R, Z_R bosons, LFV decays, observable neutron oscillations and dominant LNV decay via an extended seesaw mechanism [37]. The possibility of an LHC accessible low-mass Z' has been also investigated recently in the context of heterotic string models [38]. Another attractive aspect of non-SUSY SO(10) is rare kaon decay and neutron–antineutron oscillation, which has been discussed in a recent work with an inverse seesaw mechanism for light-neutrino masses and TeV scale Z' bosons but having much larger W_R mass not accessible to LHC [39]. The viability of the model of Ref. [32] depends on the discovery of TeV scale SUSY, TeV scale W_R, Z_R bosons and TeV scale pseudo-Dirac neutrinos. The viability of the non-SUSY model of Ref. [36] depends on the discovery of TeV scale low-mass Z_R boson and heavy pseudo Dirac neutrinos in the range 100–1200 GeV; both types of models predict a proton lifetime within the Super-K search limit. The falsifiability of the non-SUSY model of Ref. [39] depends upon any one of the following predicted observables: the TeV scale Z_R boson, dominant neutrino-less double beta decay, heavy Majorana type sterile and right-handed neutrinos, neutron oscillation and rare kaon decays. Whereas the neutrino mass generation mechanism in all these models is through a gauged inverse seesaw mechanism, our main thrust in the present work is the Type-II seesaw. A key ansatz to resolve the issue of a large mixing in the neutrino sector and small mixing in the quark sector has been suggested to be Type-II seesaw dominance [40–43] via renormalisation group evolution of quasi-degenerate neutrino masses that holds in supersymmetric quark–lepton unified theories [10,11] or SO(10) and for large values of tan β, which represents the ratio of the VEVs of up-type and down type Higgs doublets. In an interesting approach to understand neutrino mixing in SUSY theories, it has been shown [44] that the maximality of atmospheric neutrino mixing is an automatic consequence of Type-II seesaw dominance and b–τ unification that does not require quasi-degeneracy of the associated neutrino masses. A number of consequences of this approach have been explored to explain all the fermion masses and mixings by utilising Type-II seesaw, or a combination of both Type-I and Type-II seesaw [45–52] through SUSY SO(10). As a further interesting property of Type-II seesaw dominance, it has been recently shown [53–55] without using any flavour symmetry that the well-known tri-bimaximal mixing pattern for neutrino mixings is simply a consequence of rotation in the flavour space. Although several models of Type-II seesaw dominance in SUSY SO(10) have been investigated, precision gauge coupling unification is distorted in most cases.[1] All the charged fermion mass fittings in the conventional one-step breaking of SUSY GUTs including fits to the neutrino oscillation data require the left-handed triplet to be lighter than the Type-I seesaw scale. The gauge coupling evolutions, being sensitive to the quantum numbers of the LH triplet $\Delta_L(3, -2, 1)$ under an SM gauge group, tend to misalign the precision unification in the minimal scenario achieved without the lighter triplet.

Two kinds of SO(10) models have been suggested for ensuring precision gauge coupling unification in the presence of Type-II seesaw dominance. In the first type of SUSY model [57], SO(10) breaks at a very high scale, $M_U \geq 10^{17}$ GeV, to SUSY SU(5), which further breaks to the minimal supersymmetric standard model (MSSM) at the usual SUSY GUT-scale $M_U \sim 2 \times 10^{16}$ GeV. Type-II seesaw dominance is achieved by fine tuning the mass of the full SU(5) multiplet 15_H containing the $\Delta_L(3, -2, 1)$ to remain at the desired Type-II scale $M_{\Delta_L} = 10^{11}$–10^{13} GeV. Since the full multiplet 15_H is at the intermediate scale, although the evolutions of the three gauge couplings of the MSSM gauge group deflect from their original paths for $\mu > M_{\Delta_L}$, they converge exactly at the same scale M_U as the MSSM unification scale but with a slightly larger value of the GUT coupling leading to a marginal reduction of the proton-lifetime prediction compared to SUSY SU(5). In the second class of models, applicable to a non-SUSY or split-SUSY case [56], the grand unification group SO(10) breaks directly to the SM

[1] A brief review of different SUSY SO(10) models requiring Type-II seesaw, or an admixture of Type-I and Type-II for fitting fermion masses is given in Ref. [53–55]. and a brief review of distortion occurring to precision gauge coupling unification is given in Ref. [56].

gauge symmetry at the GUT-scale $M_U \sim 2 \times 10^{16}$ GeV, and by tuning the full SU(5) scalar multiplet 15_H to have degenerate masses at $M_{\Delta_L} = 10^{11}$–10^{13} GeV, the Type-II seesaw dominance is achieved. The question of precision unification is answered in this model by pulling out all the superpartner scalar components of the MSSM but by keeping all the fermionic superpartners and the two Higgs doublets near the TeV scale. In the non-SUSY case the TeV scale fermions can also be equivalently replaced by complex scalars carrying the same quantum numbers. The proton-lifetime prediction is $\tau_P(p \to e^+\pi^0) \simeq 10^{35}$ years in this model.

In the context of LR gauge theory, the Type-II seesaw mechanism was originally proposed with manifest left–right symmetric gauge group $SU(2)_L \times SU(2)_R \times U(1)_{B-L} \times SU(3)_C \times D$ ($g_{2L} = g_{2R}$) ($\equiv G_{2213D}$) where both the left- and the right-handed triplets are allowed to have the same mass scale as the LR symmetry breaking (or parity breaking) scale [58]. With the emergence of D-parity and its breaking leading to decoupling of parity and $SU(2)_R$ breakings [59,60], a new class of asymmetric LR gauge group also emerged: $SU(2)_L \times SU(2)_R \times U(1)_{B-L} \times SU(3)_C$ ($g_{2L} \neq g_{2R}$) ($\equiv G_{2213}$) where the left-handed triplet acquired a larger mass than the RH triplet leading to the Type-I seesaw dominance and suppression of Type-II seesaw in SO(10) [61]. It is possible to accommodate both types of intermediate symmetries in non-SUSY SO(10), but these models make negligible predictions for the branching ratios of charged LFV processes and they leave no other experimental signatures verifiable at low or LHC energies except $0\nu\beta\beta$ decay.

The purpose of this work is to show that in a class of models descending from non-SUSY SO(10) or from Pati–Salam gauge symmetrty, Type-II seesaw dominance at intermediate scales ($M_\Delta \simeq 10^8$–10^9 GeV) but with $M_N \sim O(1)$–$O(10)$ TeV can be realised by cancellation of the Type-I seesaw contribution along with the prediction of a Z' boson at the $\sim O(1)$–$O(10)$ TeV scale, accessible to the LHC, where $U(1)_R \times U(1)_{B-L}$ breaks spontaneously to $U(1)_Y$ through the VEV of the RH triplet component of Higgs scalar contained in 126_H that carries $B - L = -2$.

Although two-step breakings of LR gauge theory was embedded earlier in non-SUSY GUTs with low-mass Z' (for earlier work on, Z' boson in GUTs embedding two-step breaking of left-right gauge symmetry, see [33–35]), its successful compliance with neutrino oscillation data has been possible in the context of an inverse seesaw mechanism [36].

We also discuss how the Type-II seesaw contribution dominates over the linear seesaw formula. Whereas in all previous Type-II seesaw dominance models in SO(10), the RH Majorana neutrino masses have been very large and inaccessible for accelerator energies, the present model predicts these masses in the LHC accessible range. In spite of large values of the W_R boson and the doubly charged Higgs boson Δ_L^{++}, Δ_R^{++} masses, it is quite interesting to note that the model predicts a new observable contribution to $0\nu\beta\beta$ decay in the W_L–W_L channel. The key ingredients to achieve Type-II seesaw dominance by complete suppression of Type-I seesaw contribution are addition of one SO(10) singlet fermion per generation ($S_i, i = 1, 2, 3$) and utilisation of the additional Higgs representation 16_H to generate the N–S mixing term in the Lagrangian through the Higgs-Yukawa interaction. The underlying leptonic non-unitarity effects lead to substantial LFV decay branching ratios and leptonic CP-violation accessible to ongoing search experiments. We derive a new formula for the half-life of $0\nu\beta\beta$ decay as a function of the fermion singlet masses and extract lower bound on the lightest sterile neutrino mass from the existing experimental lower bounds on the half-life of different experimental groups. For certain regions of the parameter space of the model, we also find the proton lifetime for $p \to e^+\pi^0$ to be accessible to ongoing or planned experiments.

Compared to earlier existing SO(10)-based Type-II seesaw dominant models whose RH neutrino masses are in the inaccessible range and new gauge bosons are in the mass range 10^{15}–10^{17} GeV, the present model predictions on LHC scale Z', light and heavy Majorana type sterile neutrinos, RH Majorana neutrino masses in the range $\simeq$ 100–10, 000 GeV accessible to LHC in the $W_L - W_L$ channel through dilepton production, the LFV branching ratios closer to experimental limits, and dominant $0\nu\beta\beta$ decay amplitudes caused by sterile neutrino exchanges provide a rich testing ground for new physics signatures.

This paper is organised as follows. In Sect. 2. we give an outline of the model and discuss gauge coupling unification along with proton lifetime predictions. In Sect. 3 we derive a Type-II seesaw dominance formula and show how the model predicts RH neutrino masses from fits to the neutrino oscillation data. In Sect. 4 we discuss the derivation of the Dirac neutrino mass matrix from the GUT-scale fit to the fermion masses. In Sect. 5 we discuss predictions on lepton flavour violation and leptonic CP violation due to the underlying non-unitarity effects. In Sect. 6 we discuss briefly the analytic derivation of amplitudes on lepton number violation. In Sect. 7 we discuss predictions on the effective mass parameters and half-life for $0\nu\beta\beta$; we also obtain the singlet fermion mass bounds. We also indicate very briefly some plausible model applications including effects on electroweak precision observables, Z–Z' mixings, dilepton production and leptogenesis in Sect. 8. We summarise and conclude our results in Sect. 9.

2 Unification with TeV scale Z'

In this section we devise two symmetry breaking chains of non-SUSY SO(10) theory, one with LR symmetric gauge

theory with unbroken D-parity and another without D-parity at the intermediate scale. In the subsequent sections we will compare the ability of the two models to accommodate Type-II seesaw dominance to distinguish one model from the other. As necessary requirements, we introduce one SO(10)-singlet per generation ($S_i, i = 1, 2, 3$) and Higgs representations 126_H and 16_H in both models.

2.1 Models from SO(10) symmetry breaking

Different steps of symmetry breaking are given below for the following two models:

Model I

$$\begin{aligned}
\mathrm{SO}(10) &\xrightarrow{(M_U=M_P)} \mathrm{SU}(2)_L \times \mathrm{SU}(2)_R \times U(1)_{B-L} \times \mathrm{SU}(3)_C \ [G_{2213}] \\
&\xrightarrow{(M_R^+)} \mathrm{SU}(2)_L \times U(1)_R \times U(1)_{B-L} \times \mathrm{SU}(3)_C \ [G_{2113}] \\
&\xrightarrow{(M_R^0)} \mathrm{SU}(2)_L \times U(1)_Y \times \mathrm{SU}(3)_C \ [\mathrm{SM}] \\
&\xrightarrow{(M_Z)} \mathrm{SU}(3)_C \times U(1)_Q,
\end{aligned}$$

Model II

$$\begin{aligned}
\mathrm{SO}(10) &\xrightarrow{(M_U)} \mathrm{SU}(2)_L \times \mathrm{SU}(2)_R \times U(1)_{B-L} \times \mathrm{SU}(3)_C [G_{2213D}] \\
&\xrightarrow{(M_R^+=M_P)} \mathrm{SU}(2)_L \times U(1)_R \times U(1)_{B-L} \times \mathrm{SU}(3)_C \ [G_{2113}] \\
&\xrightarrow{(M_R^0)} \mathrm{SU}(2)_L \times U(1)_Y \times \mathrm{SU}(3)_C \ [\mathrm{SM}] \\
&\xrightarrow{(M_Z)} \mathrm{SU}(3)_C \times U(1)_Q.
\end{aligned}$$

In Model II, $\mathrm{SU}(2)_L \times \mathrm{SU}(2)_R \times U(1)_{B-L} \times \mathrm{SU}(3)_C \times D$ [$\equiv G_{2213D}$]($g_{2L} = g_{2R}$) is obtained by breaking the GUT-symmetry and by giving the VEV to the D-parity even singlet $(1, 1, 0, 1) \subset (1, 1, 15) \subset 210_H$ [59,60,62] where the first, the second and the third set of quantum numbers of the scalar components are under G_{2213P}, the Pati–Salam symmetry G_{224} and SO(10), respectively. As a result, the Higgs sector is symmetric below $\mu = M_U$, leading to equality between the gauge couplings $g_{2L}(M_R^+)$ and $g_{2R}(M_R^+)$. In this case the LR discrete symmetry ($\equiv$ parity) survives down to the intermediate scale, $M_{R^+} = M_P$. The second step of symmetry breaking is implemented by assigning a VEV to the neutral component of the right-handed (RH) Higgs triplet $\sigma_R(1, 3, 0, 1) \subset 45_H$ that carries $B - L = 0$. The third step of breaking to SM is carried out by assigning a VEV of $\mathcal{O}$(5–10) TeV to the G_{2113} component $\Delta_R^0(1, 1, -2, 1)$ contained in the RH triplet $\Delta_R(1, 3, -2, 1) \subset 126_H$ carrying $B - L = -2$. This is responsible for the RH Majorana neutrino mass generation $M_N = fV_R$ where $V_R = \langle \Delta_R^0 \rangle$ and f is the Yukawa coupling of $126^\dagger$ to SO(10) spinorial fermionic representation: $f\mathbf{16.16.126^\dagger_H}$. We introduce SO(10) invariant N–S mixing mass via the Yukawa interaction $y_\chi \mathbf{16.1.16^\dagger_H}$ and obtain the mixing mass $M = y_\chi V_\chi$ where $V_\chi = \langle \chi_R^0 \rangle$ by noting that under G_{2113} the submultiplet $\chi_R^0(1, 1/2, -1, 1)$ is contained in the G_{2213} doublet $\chi_R(1, 2, -1, 1) \subset 16_H$. The symmetry breaking in the last step is implemented through the SM Higgs doublet contained in the bidoublet $\phi(2, 2, 0, 1) \subset 10_H$ of SO(10). This is the minimal Higgs structure of the model, although we will utilise two different Higgs doublets $\phi_u \subset 10_{H_1}$ and $\phi_d \subset 10_{H_2}$ for fermion mass fits. In Model I, the GUT-symmetry breaks to LR gauge symmetry $G_{2213}(g_{2L} \neq g_{2R})$ in such a way that the D-parity breaks at the GUT-scale and is decoupled from $\mathrm{SU}(2)_R$ breaking, which occurs at the intermediate scale. This is achieved by giving a GUT scale VEV to the D-parity odd singlet-scalar component in $(1, 1, 0, 1)_H \subset (1, 1, 15)_H \subset 45_H$ where the first, the second and the third submultiplets are under G_{2213}, the Pati–Salam symmetry G_{224} and SO(10), respectively. In this case by adopting the D-parity breaking mechanism [59,60] in SO(10), normally the LH triplet component $\Delta_L(3, 1, -2, 1) \subset 126_H$ and the LH doublet component $\chi_L(2, 1, -1, 1) \subset 16_H$ acquire masses at the GUT-scale, while the RH triplet and RH doublet components, $\Delta_R(1, 3, -2, 1) \subset 126_H$ $\chi_R(1, 2, -1, 1) \subset 16_H$, can be made much lighter. We have noted that in the presence of a colour octet at lower scales, found to be necessary in Model I as well as in Model II, precision gauge coupling is achieved even if the parameters of the Higgs potential are tuned so as to have the LH triplet mass at intermediate scale, $M_{\Delta_L} \simeq 10^8$–10^9 GeV. The presence of $\Delta_L(3, 1, -2, 1)$ at the intermediate scale plays a crucial role in achieving Type-II seesaw dominance as will be explained in the following section. The necessary presence of lighter LH triplets in GUTs with or without vanishing $B - L$ value for physically appealing predictions was pointed out earlier in achieving observable matter–anti-matter oscillations [63,64], in the context of low-scale leptogenesis [65], and Type-II seesaw dominance in SUSY, non-SUSY and split-SUSY models [56,57], and also for TeV scale LR gauge theory originating from SUSY SO(10) grand unification [32].

2.2 Renormalisation group solutions to mass scales

In this section while safeguarding precise unification of gauge couplings at the GUT-scale, we discuss allowed solutions of renormalisation group equations (RGEs) for the mass scales M_U, M_{R^+} and M_{R^0} as a function of the mass M_C of the lighter colour octet $C_8(1, 1, 0, 8) \subset 45_H$. The Higgs scalars contributing to RG evolutions are presented in Table 1 for Model I. In Model II, in addition to the Higgs scalars shown in Table 1, the masses of the left-handed scalars $\chi_L(2, 1, -1, 1)$ and $\sigma_L(3, 1, 0, 1)$ are naturally constrained to be at $\mu = M_R^+ = M_P =$, the parity violation scale.

The renormalisation group (RG) coefficients for the minimal cases are given in Appendix A to which those due to the colour octet scalar in both models and the LH triplet Δ_L in Model I in their suitable ranges of the running scale have been added.

Table 1 Higgs scalars and their quantum numbers used in Model I in the respective ranges of mass scales. The mass of colour octet $C_8(1,0,0,8)$ has been used in the range 10^4–10^{11} GeV contributing to the variation of predicted proton lifetime discussed below in Sect. 2.3. In Model II, in addition to these scalars, the masses of the left-handed scalars $\chi_L(2,1,-1,1)$ and $\sigma_L(3,1,0,1)$ are constrained to be at $\mu = M_R^+ = M_P =$, the parity violation scale

Mass scale (μ)	Symmetry	Higgs scalars (Model I)
$M_Z - M_R^0$	G_{213}	$\Phi(2,1,1)$
$M_R^0 - M_R^+$	G_{2113}	$\Phi_1(2,1,0,1)$, $\Phi_2(2,1,0,1)$, $\chi_R(1,1/2,-1,1)$, $\Delta_R(1,1,-2,1)$, $C_8(1,0,0,8)$
$M_R^+ - M_U$	G_{2213}	$\Phi_1(2,2,0,1)$, $\Phi_2(2,2,0,1))$, $\chi_R(1,2,-1,1)$, $\Delta_R(1,3,-2,1)$, $\Delta_L(3,1,-2,1)$, $C_8(1,0,0,8)$, $\sigma_R(1,3,0,1)$

Table 2 Allowed values of mass scales as solutions of RGEs for gauge couplings for Model I with fixed value of the LH triplet mass $M_\Delta = 10^8$ GeV

M_R^0 (TeV)	M_C (GeV)	M_R^+ (GeV)	M_G (GeV)	α_G^{-1}	τ_p (years)
10	$10^{4.5}$	10^9	$10^{16.9}$	41.1	5.4×10^{39}
10	10^5	$10^{8.9}$	$10^{16.74}$	41.4	1.1×10^{39}
10	10^7	10^9	$10^{16.4}$	41.7	8.4×10^{37}
10	$10^{10.9}$	$10^{9.7}$	$10^{15.63}$	41.9	3.2×10^{34}
5	$10^{7.8}$	$10^{8.8}$	$10^{16.4}$	41.5	9×10^{37}

Model I:

As shown in Table 2 for Model I, with $M_{\Delta_L} = 10^8$ GeV the G_{2213} symmetry is found to survive down to $M_{R^+} = (10^8$–$10^{10})$ GeV with larger or smaller unification scale depending upon the colour octet mass. In particular we note one set of solutions,

$$M_{R^0} = 10\,\text{TeV},\ M_{R^+} = 10^{9.7}\text{GeV},\ M_U = 10^{15.62}\text{GeV},$$
$$M_{\Delta_L} = 10^8\ \text{GeV},\ M_C = 10^{10.9}\text{GeV}. \quad (4)$$

As explained in the following sections, this set of solutions are found to be attractive both from the prospects of achieving Type-II seesaw dominance and detecting proton decay at Hyper-Kamiokande. with $M_U = 6.5 \times 10^{15}$ GeV when the colour octet mass is at $M_C \sim 10^{11}$ GeV. As discussed below, the proton lifetime in this case is closer to the current experimental limit. With the allowed values of $M_{R^0} = (5$–$10)$ TeV, this model also predicts $M_{Z'} \simeq (1.2$–$3.5)$ TeV in the accessible range of the LHC. As discussed in Sect. 3, because of the low mass of the Z' boson associated with TeV scale VEV of V_R, the Type-II seesaw mechanism predicts RH neutrino masses which can be testified at the LHC or future high energy accelerators.

The RG evolution of gauge couplings for the set of mass scales given in Eq. (4) is presented in Fig. 1, showing clearly the unification of the four gauge couplings of the G_{2213} intermediate gauge symmetry.

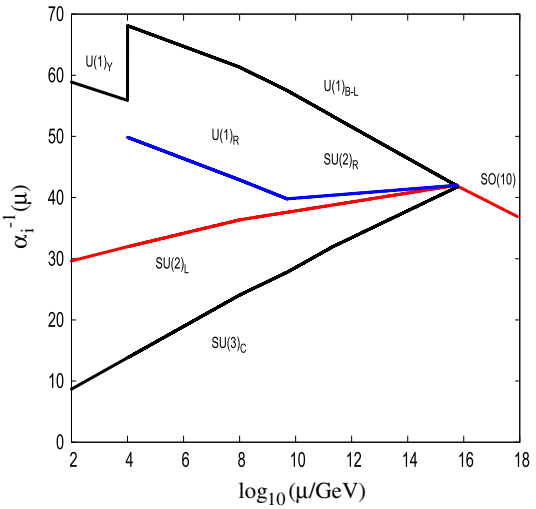

Fig. 1 Two-loop gauge coupling unification in the SO(10) symmetry breaking chain with $M_U = 10^{15.62}$ GeV and $M_R^+ = 10^{9.7}$, $M_{\Delta_L} = 10^8$ GeV with a low-mass Z' boson at $M_R^0 = 10$ TeV for Model I

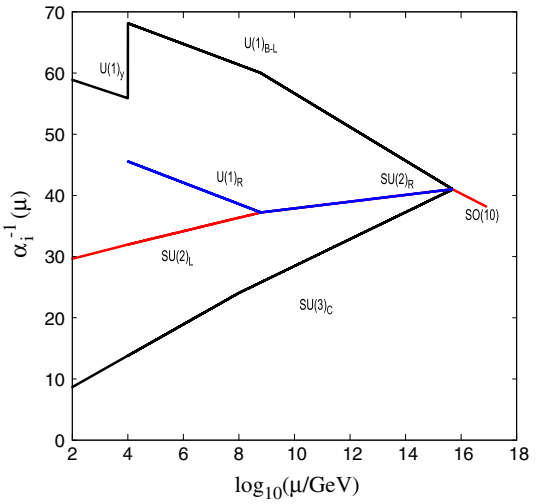

Fig. 2 Two-loop gauge coupling unification in the SO(10) symmetry breaking chain with $M_U = 10^{15.62}$ GeV and $M_{R^+} = 10^{8.7}$ GeV with a low-mass Z' boson at $M_R^0 = 10$ TeV for Model II

Model II: In addition to the Higgs scalars of Table 1, this model has the masses of left-handed scalars $\chi_L(2,1,-1,1)$ and $\sigma_L(3,1,0,1)$ naturally at $\mu = M_R^+ = M_P =$, the parity violation scale. As shown in Table 3 for Model II, the G_{2213D} symmetry is found to survive down to $M_{R^+} = M_P = 10^{8.2}$ GeV with $M_U = 6.5 \times 10^{15}$ GeV when the colour octet mass is at $M_C = 10^8$ GeV. As discussed below, the proton lifetime in this case is closer to the current experimental limit.

One example of RG evolution of gauge couplings is shown in Fig. 2 for $M_{R^0} = 10$ GeV, $M_{R^+} = 10^{8.7}$ GeV, $M_C = 10^8$ GeV and $M_U = 6.5 \times 10^{15}$ GeV. Clearly the fig-

Table 3 Allowed mass scales as solutions of renormalisation group equations for Model II as described in the text

M_R^0 (TeV)	M_C (GeV)	M_R^+ (GeV)	M_G (GeV)	α_G^{-1}	τ_p (years)
10	$10^{4.5}$	$10^{7.886}$	$10^{16.15}$	40.25	4.3×10^{36}
10	$10^{5.5}$	$10^{7.89}$	$10^{16.04}$	40.64	1.6×10^{36}
10	10^{8}	$10^{8.789}$	$10^{15.62}$	41.49	3.9×10^{34}
10	$10^{8.5}$	$10^{8.8}$	$10^{15.5}$	41.69	1.12×10^{34}
5	$10^{5.8}$	$10^{7.2}$	$10^{15.83}$	41.15	2.3×10^{35}

ure shows a precise unification of the three gauge couplings of the intermediate gauge symmetry G_{2213P} at the GUT-scale. For all other solutions given in Table 3, the RG evolutions and unification of the gauge couplings are similar. In both models, with the allowed values of $M_{R^+} \gg M_{R^0} = 5$–10 TeV, the numerical values of the gauge couplings g_{2L}, g_{1R} and g_{B-L} predict [66–68]

$$M_{Z'} = (1.2\text{—}3.5)\text{TeV}. \tag{5}$$

2.3 Proton-lifetime prediction

In this section we discuss predictions on the proton lifetimes in the two models and compare them with the current Super-Kamiokande limit and reachable limits by future experiments such as the Hyper-Kamiokande [69–72]. Currently, the Super-Kamiokande detector has reached the search limit

$$(\tau_p)_{\text{expt.}}(p \to e^+\pi^0) \geq 1.4 \times 10^{34} \text{ years}. \tag{6}$$

The proposed 5.6 Megaton years Cherenkov water detector at Hyper-Kamiokande is expected to probe a lifetime [69–72]

$$(\tau_p)_{\text{Hyper-K.}}(p \to e^+\pi^0) \geq 1.3 \times 10^{35} \text{ years}. \tag{7}$$

The width of the proton decay for $p \to e^+\pi^0$ is expressed as [73–75]

$$\Gamma(p \to e^+\pi^0) = \left(\frac{m_p}{64\pi f_\pi^2}\right) \times \left(\frac{{g_G}^4}{{M_U}^4}\right) \times |A_L|^2 |\bar{\alpha_H}|^2 (1 + D + F)^2 \times R, \tag{8}$$

where $R = [(A_{SR}^2 + A_{SL}^2)(1 + |V_{ud}|^2)^2]$ for SO(10), $V_{ud} = 0.974$ = is the $(1, 1)$ element of V_{CKM} for quark mixings, $A_{SL}(A_{SR})$ is the short-distance renormalisation factor in the left (right) sectors and $A_L = 1.25$ = the long distance renormalisation factor. M_U is the degenerate mass of the 24 superheavy gauge bosons in SO(10), $\bar{\alpha}_H$ the hadronic matrix element, m_p the proton mass = 938.3 MeV, f_π the pion decay constant, 139 MeV, and the chiral Lagrangian parameters are $D = 0.81$ and $F = 0.47$. With $\alpha_H = \bar{\alpha_H}(1 + D + F) = 0.012\,\text{GeV}^3$ obtained from lattice gauge theory computations, we get $A_R \simeq A_L A_{SL} \simeq A_L A_{SR} \simeq 2.726$ for both models. The expression for the inverse decay rates for the models is expressed as

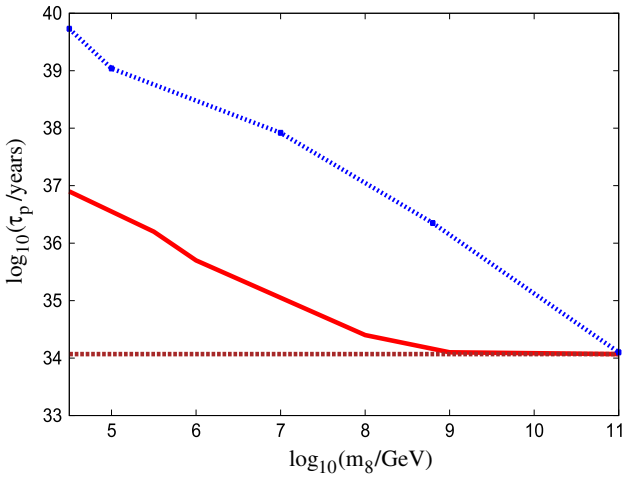

Fig. 3 Variation of proton lifetime as a function of color octet mass M_C for Model I (*upper curve*) and Model II (*lower curve*). The *horizontal line* is the present experimental limit

$$\tau_p = \Gamma^{-1}(p \to e^+\pi^0) = \frac{64\pi f_\pi^2}{m_p}\left(\frac{{M_U}^4}{{g_G}^4}\right) \times \frac{1}{|A_L|^2 |\bar{\alpha_H}|^2 (1 + D + F)^2 \times R}, \tag{9}$$

where the factor $F_q = 2(1 + |V_{ud}|^2)^2 \simeq 7.6$ for SO(10). Now using the given values of the model parameters the predictions on the proton lifetimes for both models are given in Tables 2 and 3. We find that for proton-lifetime predictions accessible to Hyper-Kamiokande detector, it is necessary to have an intermediate value of the color octet mass $M_C \geq 10^{8.6}$GeV in Model II and $M_C \geq 10^{10.8}$GeV in Model I. The predicted proton lifetime as a function of the colour octet mass is shown in Fig. 3 both for Model I and for Model II. These analyses suggest that a low colour octet mass in the TeV scale and observable proton lifetime within the Hyper-Kamiokande limit are mutually exclusive. If LHC discovers a colour octet within its achievable energy range, proton decay searches would need far bigger detector than the Hyper-K detector. On the other hand the absence of a colour octet at the LHC would still retain the possibility of observing proton decay within the Hyper-K limit.

3 Type-II seesaw dominance

In this section we discuss prospects of having a Type-II seesaw dominated neutrino mass formula in the two SO(10)-based models discussed in Sect. 2.

3.1 Derivation of Type-II seesaw formula

We have added to the usual spinorial representations $16_{F_i}(i = 1,2,3)$ for fermion representations in SO(10) and one fermion singlet per generation $S_i(i = 1,2,3)$. The G_{2213} symmetric Yukawa Lagrangian descending from SO(10) symmetry can be written as

$$\mathcal{L}_{\rm Yuk} = \sum_{i=1,2} Y_i^{\ell}\left(\overline{\psi}_L\,\psi_R\,\Phi_i\right) + f(\,\psi_R^c\,\psi_R\Delta_R + \psi_L^c\,\psi_L\Delta_L) + y_\chi\,\left(\overline{\psi}_R\,S\,\chi_R + \overline{\psi}_L\,S\,\chi_L\right) + (\text{h.c.})\,, \tag{10}$$

where $\Phi_{1,2} \subset 10_{H_1,H_2}$ are two bidoublets, $(\Delta_L, \Delta_R) \subset 126_F$ and $(\chi_L, \chi_R) \subset 16_H$. As discussed in Sect. 2, the spontaneous breaking of $G_{2213} \longrightarrow G_{2113}$ takes place by the VEV of the RH triplet $\sigma_R(1,3,0,1) \subset 45_H$ carrying $B-L=0$, which does not generate any fermion mass term. As we discuss below, when the Higgs scalar Φ_i, Δ_R and χ_R acquire VEVs spontaneous symmetry breakings leading to $G_{2113} \longrightarrow SM \longrightarrow U(1)_{em} \times SU(3)_C$ occur and generate an N–S mixing mass term $M = y_\chi\langle\chi_R^0\rangle$ by the induced VEVs. In addition, $v_{\chi_L} = \langle\chi_L^0\rangle$ and $v_L = \langle\Delta_L^0\rangle$ are automatically generated even though the LH doublet χ_L and the RH triplet Δ_L are assigned vanishing VEVs directly. In models with the inverse seesaw [76,77] or extended seesaw [36,37,78–82] mechanisms, a bare mass term of the singlet fermions $\mu_S S^T S$ occurs in the Lagrangian. Being unrestricted as a gauge singlet mass term in the Lagrangian, determination of its value has been left to phenomenological analyses in neutrino physics. Larger values of the parameter near the GUT-Planck scale [83] or at the intermediate scale [84,85] have also been exploited. On the other hand, fits to the neutrino oscillation data through an inverse seesaw formula by a number of authors have been shown to require much smaller values of μ_S [32,36,37,78] (see, for instance [86]), [87–91]. Even phenomenological implications of its vanishing value have been investigated recently in the presence of other non-standard and non-vanishing fermion masses [92–95] in the 9×9 mass matrix. Very small values of μ_S are justified on the basis of 't Hooft's naturalness criterion, representing a mild breaking of global lepton number symmetry of the SM [96]. While we consider the implication of this term later in this section, at first we discuss the emerging neutrino mass matrix by neglecting it. In addition to the VEVs discussed in Sect. 2 for gauge symmetry breaking at different stages, we assign the VEV to the neutral component of RH Higgs doublet of 16_H with $\langle\chi_R(1,1/2,-1/2,1)\rangle = V_\chi$ in order to generate an N–S mixing mass term $\mathrm{M}\overline{N}S$ between the RH neutrino and the sterile fermion where we have the 3×3 matrix $\mathrm{M} = y_\chi V_\chi$. We define the other 3×3 mass matrices $M_D = Y^{(1)}v_u$ and $M_N = fV_R$. We also include induced small contributions to the VEV of the LH Higgs triplet $v_L = \langle\Delta_L(3,0,-2,1)\rangle$ and the LH Higgs doublet $v_{\chi_L} = \langle\chi_L(2,0,-2,1)\rangle$ leading to the possibilities ν–S mixing with $M_L = y_\chi v_{\chi_L}$ and the induced Type-II seesaw contribution to LH neutrino masses $m_\nu^{II} = fv_L$ given in Eq. (20). The induced VEVs are shown in the left and right panels of Fig. 4. We have also derived them by actual potential minimisation, which agrees with the diagrammatic contribution. Including the induced VEV contributions, the mass term due to the Yukawa Lagrangian can be written as

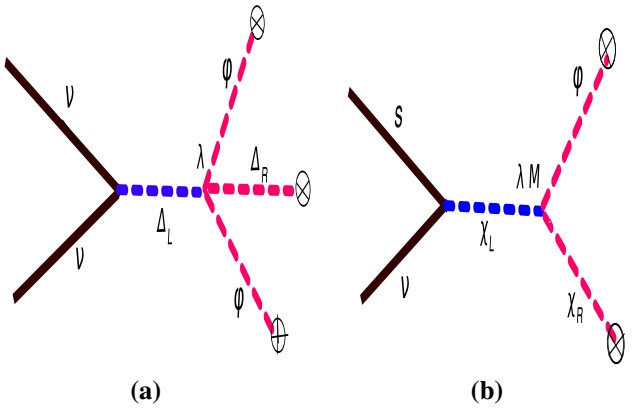

Fig. 4 Feynman diagrams for induced contributions to VEVs of the LH triplet (diagram **a**) and the LH doublet (diagram **b**) in Model I and Model II

$$\mathcal{L}_{\rm mass} = (M_D\overline{\nu}N + \frac{1}{2}M_N N^T N + M\overline{N}S + M_L\overline{\nu}S + h.c) + m_\nu^{II}\nu^T\nu. \tag{11}$$

In the (ν, S, N^C) basis the generalised form of the 9×9 neutral fermion mass matrix after electroweak symmetry breaking can be written as

$$\mathcal{M} = \begin{pmatrix} m_\nu^{II} & M_L & M_D \\ M_L^T & 0 & M^T \\ M_D^T & M & M_N \end{pmatrix}, \tag{12}$$

where $M_D = Y\langle\Phi\rangle$, $M_N = fv_R$, $\mathrm{M} = y_\chi\langle\chi_R^0\rangle$, $M_L = y_\chi\langle\chi_L^0\rangle$ and we have used $\mu_s = 0$. In this model the symmetry breaking mechanism and the VEVs are such that $M_N > M \gg M_D$. The RH neutrino mass being the heaviest fermion mass scale in the Lagrangian, this fermion is at first integrated out leading to the effective Lagrangian at lower scales [65,97–101],

$$
\begin{aligned}
-\mathcal{L}_{\rm eff} &= \left(m_\nu^{II} + M_D \frac{1}{M_N} M_D^T\right)_{\alpha\beta} \nu_\alpha^T \nu_\beta \\
&+ \left(M_L + M_D \frac{1}{M_N} M^T\right)_{\alpha m} \left(\overline{\nu_\alpha} S_m + \overline{S_m} \nu_\alpha\right) \\
&+ \left(M \frac{1}{M_N} M^T\right)_{mn} S_m^T S_n . \qquad (13)
\end{aligned}
$$

Whereas the heaviest RH neutrino mass matrix M_N separates out trivially, the other two 3×3 mass matrices $\mathcal{M}_\nu$ and m_S are extracted through various steps of block diagonalisation [37].The details of the various steps are given in Appendix B and the results are

$$
\begin{aligned}
\mathcal{M}_\nu &= m_\nu^{II} + \left(M_D M_N^{-1} M_D^T\right) - (M_D M_N^{-1} M_D^T) \\
&+ M_L (M^T M_N^{-1} M)^{-1} M_L^T \\
&- M_L (M^T M_N^{-1} M)^{-1} (M^T M_N^{-1} M_D^T) \\
&- (M_D M_N^{-1} M)(M^T M_N^{-1} M)^{-1} M_L^T , \qquad (14) \\
m_s &= -M M_N^{-1} M^T + \cdots . \\
m_N &= M_N .
\end{aligned}
$$

From the first of the above three equations, it is clear that the Type-I seesaw term cancels out [65,97–101] with another of opposite sign resulting from block diagonalisation. Then the generalised form of the light-neutrino mass matrix turns out to be

$$
\begin{aligned}
\mathcal{M}_\nu = \; & f v_L + M_L M^{-1} M_N (M^T)^{-1} M_L^T \\
& - [M_L M_D^T M^{-1} + M_L^T M_D (M^T)^{-1}] . \qquad (15)
\end{aligned}
$$

With $M_L = y_\chi v_{\chi_L}$, which induces ν–S mixing, the second term in this equation is the double seesaw formula and the third term is the linear seesaw formula, which are similar to those derived earlier [84,85].

From the Feynman diagrams, the analytic expressions for the induced VEVs are

$$
v_L \sim \frac{V_R}{M_{\Delta_L}^2} \left(\lambda_1 v_1^2 + \lambda_2 v_2^2\right) , \qquad (16)
$$

$$
\begin{aligned}
v_{\chi_L} &\sim \frac{V_\chi}{M_{\chi_L}^2} \left(\lambda_1' M_1' v_1 + \lambda_2' M_2' v_2\right) , \\
&= C_\chi \frac{V_\chi M_{R^+} v_{wk}}{M_{\chi_L}^2} , \qquad (17)
\end{aligned}
$$

where $v_{wk} \sim 100\,\text{GeV}$, and

$$
C_\chi = \frac{\left(\lambda_1' M_1' v_1 + \lambda_2' M_2' v_2\right)}{(M_{R^+} v_{wk})} . \qquad (18)
$$

In Eq. (17), $v_i (i = 1, 2)$ are the VEVs of two electroweak doublets each originating from separate $10_H \subset SO(10)$ as explained in the following section, and M_1', M_2' are Higgs trilinear coupling masses which are normally expected to be of order M_{R^+}. In both models $V_R = 5$–10 TeV and $V_\chi \sim$ 300–1000 GeV. Similar expressions as in Eq. (17) are also obtained by minimisation of the scalar potential.

3.2 Suppression of linear seesaw and dominance of Type-II seesaw

Now we discuss how a linear seesaw term is suppressed without fine tuning of certain parameters in Model I but with fine tunning of the same parameters in Model II. The expression for the neutrino mass is given in Eq. (15) where the first, the second and the third terms are Type-II seesaw, double seesaw and linear seesaw formulas for the light-neutrino masses. Out of these, for all parameters allowed in both models (Model I and Model II), the double seesaw term will be found to be far more suppressed compared to the other two terms. Therefore we now discuss how the linear seesaw term is suppressed compared to the Type-II seesaw term allowing the dominance of the latter. In Model I, gauge coupling unification has been achieved such that $M_P = M_{\chi_L} \sim M_U \geq 10^{15.6}\,\text{GeV}$, $M_{\Delta_L} = 10^8\,\text{GeV}$ where $M_1' \sim M_2' \sim M_{R^+} \sim 10^9\,\text{GeV}$. Using these masses in Eq. (15), we find that even with $C_\chi \sim 0.1$–1.0

$$
\begin{aligned}
v_{\chi_L} &\sim 10^{-18}\,\text{eV}\text{–}10^{-17}\,\text{eV}, \\
v_L &\simeq 0.1\,\text{eV} - 0.5\,\text{eV}. \qquad (19)
\end{aligned}
$$

Such induced VEVs in Model I suppress the second and the third terms in Eq. (15) making the model quite suitable for Type-II seesaw dominance although the Model II needs fine tuning in the induced contributions to the level of $C_\chi \leq 10^{-5}$ as discussed below.

In Model II, $M_{\Delta_L} \sim M_{\chi_L} \sim M_P \sim 10^9\,\text{GeV}$, and without any fine tuning of the parameters in Eq. (16), we obtain $v_L \sim 10^{-10}\,\text{GeV}$. From Eq. (17) we get $v_{\chi_L} \sim C_\chi \times 10^{-6}\,\text{GeV} \sim 10^{-7}\,\text{GeV}$ for $C_\chi \sim 0.1$. With $(M_D)_{(3,3)} \leq 100\,\text{GeV}$ and $\frac{M_D}{M} \simeq 0.1$–1, the most dominant third term in Eq. (15) gives $M_\nu \geq 10^{-8}\,\text{GeV}$. This shows that fine tuning is needed in the parameters occurring to reduce $C_\chi \leq 10^{-5}$ to suppress linear seesaw and permit Type-II seesaw dominance in Model II whereas the Type-II seesaw dominance is achieved in Model I with $C_\chi \simeq 0.1$–1.0 without requiring any such fine tuning. In what follows we will utilise the Type-II seesaw dominated neutrino mass formula to study neutrino physics,[2] neutrinoless double beta decay and lepton flavour violations in the context of Model I although they are similar in Model II

[2] Following a similar block diagonalisation procedure to Appendix B, but in the presence of $\mu_S S^T S$ in the Yukawa Lagrangian with mass ordering $M_N > M >> M_D, \mu_S$ results in the appearance of the inverse seesaw part of the full neutrino mass matrix, $\mathcal{M}_\nu' = f v_L + (\frac{M_D}{M}) \mu_S (\frac{M_D}{M})^T$. Although we plan to investigate the implications of this formula in a future work, for the present purpose we assume $\mu_S \simeq 0$ such that Type-II seesaw dominance prevails.

subject to the fine tuning constraint on C_χ. Thus the light-neutrino mass is dominated by the Type-II seesaw term

$$\mathcal{M}_\nu \simeq f v_L. \tag{20}$$

3.3 Right-handed neutrino mass prediction

Global fits to the experimental data [102–105] on neutrino oscillations have determined the mass squared differences and mixing angles at 3σ level,

$$\begin{aligned} &\sin^2\theta_{12} = 0.320, \quad \sin^2\theta_{23} = 0.427, \\ &\sin^2\theta_{13} = 0.0246, \ \ \delta_{CP} = 0.8\pi, \\ &\Delta m^2_{\rm sol} = 7.58\times 10^{-5}{\rm eV}^2, \\ &|\Delta m_{\rm atm}|^2 = 2.35\times 10^{-3}{\rm eV}^2. \end{aligned} \tag{21}$$

For normally hierarchical (NH), inverted hierarchical (IH) and quasi-degenerate (QD) patterns, the experimental values of mass squared differences can be fitted by the following values of the light neutrino masses:

$$\begin{aligned} \hat{m}_\nu &= (0.00127, 0.008838, 0.04978)\ {\rm eV}\ ({\rm NH}) \\ &= (0.04901, 0.04978, 0.00127)\ {\rm eV}\ ({\rm IH}) \\ &= (0.2056, 0.2058, 0.2)\ {\rm eV}\ ({\rm QD}) \end{aligned} \tag{22}$$

We use the diagonalising Pontecorvo–Maki–Nakagawa–Sakata (PMNS) matrix. The $U_{\rm PMNS}$ matrix is given by

$$\begin{pmatrix} c_{13}c_{12} & c_{13}s_{12} & s_{13}e^{-i\delta} \\ -c_{23}s_{12} - c_{12}s_{13}s_{23}e^{i\delta} & c_{12}c_{23} - s_{12}s_{13}s_{23}e^{i\delta} & s_{23}c_{13} \\ s_{12}s_{23} - c_{12}c_{23}s_{13}e^{i\delta} & -c_{12}s_{23} - s_{12}s_{13}c_{23}e^{i\delta} & c_{13}c_{23} \end{pmatrix}, \tag{23}$$

and we determine it using mixing angle and the leptonic Dirac phase from Eq. (21)

$$U_{\rm PMNS} = \begin{pmatrix} 0.814 & 0.55 & -0.12 - 0.09i \\ -0.35 - 0.049i & 0.67 - 0.034i & 0.645 \\ 0.448 - 0.057i & -0.48 - 0.039i & 0.74 \end{pmatrix}. \tag{24}$$

Now inverting the relation $\hat{m}_\nu = U^\dagger_{\rm PMNS}\mathcal{M}_\nu U^*_{\rm PMNS}$ where $\hat{m}_\nu$ is the diagonalised neutrino mass matrix, we determine $\mathcal{M}_\nu$ for three different cases and further determine the corresponding values of the f matrix using $f = \mathcal{M}_\nu/v_L$ where we use the predicted value of $v_L = 0.1$ eV. Noting that $M_N = fV_R = \mathcal{M}_\nu V_R/v_L$, we have also derived the eigenvalues of the RH neutrino mass matrix $\hat{M}_{N_i}$ as the positive square root of the i^{th} eigenvalue of the Hermitian matrix $M_N^\dagger M_N$. We have the following solutions:

NH

$$f = \begin{pmatrix} 0.117 + 0.022i & -0.124 - 0.003i & 0.144 + 0.025i \\ -0.124 - 0.003i & 0.158 - 0.014i & -0.141 + 0.017i \\ 0.144 + 0.025i & -0.141 + 0.017i & 0.313 - 0.00029i \end{pmatrix}, \tag{25}$$

$$|\hat{M}_N| = {\rm diag}(160, 894, 4870)\ {\rm GeV}. \tag{26}$$

IH

$$f = \begin{pmatrix} 0.390 - 0.017i & 0.099 + 0.01i & -0.16 + 0.05i \\ 0.099 + 0.01i & 0.379 + 0.02i & 0.176 + 0.036i \\ -0.16 + 0.05i & 0.176 + 0.036i & 0.21 - 0.011i \end{pmatrix}, \tag{27}$$

$$|\hat{M}_N| = {\rm diag}(4880, 4910, 131)\ {\rm GeV}. \tag{28}$$

QD

$$f = \begin{pmatrix} 2.02 + 0.02i & 0.0011 + 0.02i & -0.019 + 0.3i \\ 0.0011 + 0.02i & 2.034 + 0.017i & 0.021 + 0.21i \\ -0.019 + 0.3i & 0.021 + 0.21i & 1.99 - 0.04i \end{pmatrix}. \tag{29}$$

For $v_L = 0.1$ eV, we have

$$|\hat{M}_N| = {\rm diag}(21.46, 20.34, 18.87)\ {\rm TeV}, \tag{30}$$

but for $v_L = 0.5$ eV we obtain

$$|\hat{M}_N| = {\rm diag}(4.3, 4.08, 3.77)\ {\rm TeV}. \tag{31}$$

These RH neutrino masses predicted with $v_L = 0.1$ eV for the NH and IH cases and with $v_L = 0.5$ eV for the QD case are clearly verifiable by the LHC.

4 The Dirac neutrino mass matrix

The Dirac neutrino mass matrix which has a quark–lepton symmetric origin [10,11] plays a crucial role in the predictions of lepton flavour violations (LFVs) [32,36] as well as lepton number violations (LNVs) as pointed out very recently [37,78]. The determination of the Dirac neutrino mass matrix $M_D(M_{R^0})$ at the TeV seesaw scale is done; it was discussed in [36,106–108].

4.1 Extrapolation to the GUT-scale

The RG extrapolated values at the GUT-scale are, with $\mu = {\rm M_{GUT}}$,

$$\begin{aligned} &m^0_e = 0.00048\ {\rm GeV}, m^0_\mu = 0.0875\ {\rm GeV}, m^0_\tau = 1.8739\ {\rm GeV}, \\ &m^0_d = 0.0027\ {\rm GeV}, m^0_s = 0.0325\ {\rm GeV}, m^0_b = 1.3373\ {\rm GeV}, \\ &m^0_u = 0.001\ {\rm GeV}, m^0_c = 0.229\ {\rm GeV}, m^0_t = 78.74\ {\rm GeV}, \end{aligned} \tag{32}$$

The $V^0_{\rm CKM}$ matrix at the GUT-scale is given by

$$V^0_{\rm CKM} = \begin{pmatrix} 0.97 & 0.22 & -0.0003 - 0.003i \\ -0.22 - 0.0001i & 0.97 & 0.036 \\ 0.008 - 0.003i & -0.035 + 0.0008i & 0.99 \end{pmatrix}. \tag{33}$$

For fitting the charged fermion masses at the GUT-scale, in addition to the two complex $10_{H_{1,2}}$ representations with their respective Yukawa couplings $Y_{1,2}$, we also use the higher-dimensional operator [32,36]

$$\frac{\kappa_{ij}}{M_G^2} \mathbf{16_i 16_j 10_H 45_H 45_H}. \tag{34}$$

In the above equation the product of three Higgs scalars acts as an effective $126^\dagger_H$ operator [32]. With $M_G \simeq M_{Pl}$ or $M \simeq M_{\rm string}$, this is suppressed by $(M_U/M_G)^2 \simeq 10^{-3}$–$10^{-5}$ for a GUT-scale VEV of 45_H. Then the formulas for different charged fermion mass matrices are

$$\begin{aligned} &M_u = G_u + F, \quad M_d = G_d + F, \\ &M_e = G_d - 3F, \quad M_D = G_u - 3F. \end{aligned} \tag{35}$$

Following the procedure given in [36], the Dirac neutrino mass matrix at the GUT-scale is found to be

$$M_D(M_{R^0}) = \begin{pmatrix} 0.014 & 0.04 - 0.01i & 0.109 - 0.3i \\ 0.04 + 0.01i & 0.35 & 2.6 + 0.0007i \\ 0.1 + 0.3i & 2.6 - 0.0007i & 79.20 \end{pmatrix} \text{GeV}. \tag{36}$$

5 Lepton flavour violation

In the present non-SUSY SO(10) models, even though the neutrino masses are governed by high scale Type-II seesaw formula, the essential presence of singlet fermions that implement the Type-II seesaw dominance by cancelling out the Type-I seesaw contribution gives rise to experimentally observable LFV decay branching ratios through their loop mediation. The heavier RH neutrinos in this model, being in the range of ∼1–10 TeV mass, also contribute, but less significantly than the singlet fermions. The charged current weak interaction Lagrangian in this model can be written in the generalised form.

5.1 Estimation of non-unitarity matrix

Using the flavour basis, the general form of the charged current weak interaction Lagrangian including both $V \pm A$ currents in Model I and Model II is

$$\mathcal{L}_{\rm CC} = -\frac{1}{\sqrt{2}} \sum_{\alpha=e,\mu,\tau} \left[g_{2L} \bar{\ell}_{\alpha\, L}\, \gamma_\mu \nu_{\alpha\, L}\, W_L^\mu + g_{2R} \bar{\ell}_{\alpha\, R}\, \gamma_\mu N_{\alpha\, R}\, W_R^\mu \right] + \text{h.c.} \tag{37}$$

In both models, the $W_R^\pm$ bosons and the doubly charged Higgs scalars, both left-handed (LH) and right-handed (RH), are quite heavy with $M_{W_R} \sim M_\Delta \simeq 10^8$–$10^9$ GeV. These make negligible contributions arising out of the RH current effects and Higgs exchange effects on LFV or LNV decay amplitudes. In the two models considered here, the flavour eigenstate of any LH neutrino ν can be represented in terms of the mass eigenstates ν_i, S_i and N_i. From details of the model parametrisation discussed in Sects. 3–5, we have found the corresponding mixing matrices with active neutrinos, $\mathcal{V}^{\nu N} = M_D/M_N \equiv X_N$ and $\mathcal{V}^{\nu S} = M_D/M \equiv X_S$,

$$\begin{aligned} &\nu = \mathcal{N}\nu_i + \mathcal{V}^{\nu N} N_i + \mathcal{V}^{\nu S} S_i, \\ &\mathcal{N} \simeq [1 - (\eta^N + \eta^S)] U_{\rm PMNS}, \\ &\eta^N = (X_N . X_N^\dagger)/2, \\ &\eta^S = (X_S . X_S^\dagger)/2. \end{aligned} \tag{38}$$

These mixings modify the standard weak interaction Lagrangian in the LH sector by small amounts but they could be in the experimentally accessible range (see, for instance [109]). In the LH sector the charged current weak interaction Lagrangian is

$$\mathcal{L}_{\rm CC} = -\frac{g_{2L}}{\sqrt{2}} W_\mu \bar{e} \gamma^\mu P_L \left(\mathcal{N}\nu_i + \mathcal{V}^{\nu N} N_i + \mathcal{V}^{\nu S} S_i \right) + h.c. \tag{39}$$

The implications of these terms for LFV and LNV effects have been discussed below. From Eq. (38) it is clear that $\mathcal{N}$ is non-unitary. We assume the N–S mixing matrix M to be diagonal for the sake of simplicity and economy of parameters,

$$M = \text{diag}\,(M_1, M_2, M_3). \tag{40}$$

Note that the non-unitarity deviation is characterised by $\eta = \eta^S + \eta^N$, which in the limit $M_N >> M$ turns out to be

$$\begin{aligned} &\eta \simeq \eta^S = \frac{1}{2} X_S . X_S^\dagger = M_D M^{-2} M_D^\dagger, \\ &\eta_{\alpha\beta} = \frac{1}{2} \sum_{k=1,2,3} \frac{M_{D_{\alpha k}} M^*_{D_{\beta k}}}{M_k^2}. \end{aligned} \tag{41}$$

For the degenerate case, $M_i = M_{\rm Deg} (i = 1, 2, 3)$, gives

$$\eta = \frac{1\text{GeV}^2}{M^2_{\rm Deg}} \times \begin{pmatrix} 0.0394 & 0.146 - 0.403i & 4.17 - 11.99i \\ 0.146 + 0.403i & 3.602 & 105.8 - 0.002i \\ 4.173 + 11.9i & 105.805 + 0.002i & 3139.8 \end{pmatrix}. \tag{42}$$

For the general non-degenerate case of M, we saturate the upper bound $|\eta_{\tau\tau}| < 2.7 \times 10^{-3}$ [110–113] to derive

$$\frac{1}{2}\left[\frac{0.1026}{M_1^2}+\frac{7.0756}{M_2^2}+\frac{6762.4}{M_3^2}\right]=2.7\times 10^{-3}. \quad (43)$$

By inspection, this equation gives the lower bounds

$$M_1 > 4.35\ \text{GeV},\ M_2 > 36.2\ \text{GeV}, M_3 > 1120\ \text{GeV}, \quad (44)$$

and for the degenerate case $M_{\text{Deg}} = 1213$ GeV. For the partially degenerate case of $M_1 = M_2 \neq M_3$, the solutions can be similarly derived as in Ref. [36] and one example is $M(100, 100, 1319.67)$ GeV.

5.2 Branching ratio and CP violation

One of the most important outcomes of non-unitarity effects is expected to become manifest through ongoing experimental searches for LFV decays such as $\tau \to e\gamma$, $\tau \to \mu\gamma$, $\mu \to e\gamma$. In these models the RH neutrinos and the singlet fermions contribute to the branching ratios [32,36,114–120]. Because of the condition $M_N >> M$, neglecting the RH neutrino exchange contribution compared to the sterile fermion singlet contributions, our estimations for the different cases of the M values are presented below. These values are many orders larger than the standard non-SUSY contributions and are accessible to ongoing or planned searches [121–126]. For the degenerate case

$$\begin{aligned}\Delta\mathcal{J}^{12}_{e\mu} &= -\,2.1\times 10^{-6},\\ \Delta\mathcal{J}^{23}_{e\mu} &= -\,2.4\times 10^{-6},\\ \Delta\mathcal{J}^{23}_{\mu\tau} &= 1.4\times 10^{-4},\\ \Delta\mathcal{J}^{31}_{\mu\tau} &= 1.2\times 10^{-4},\end{aligned} \quad (45)$$

we have the predicted values of the branching ratios

$$\begin{aligned}\text{BR}(\mu\to e\gamma) &= 6.43\times 10^{-17},\\ \text{BR}(\tau\to e\gamma) &= 8.0\times 10^{-16},\\ \text{BR}(\tau\to \mu\gamma) &= 2.41\times 10^{-12}.\end{aligned} \quad (46)$$

Because of the presence of non-unitarity effects in the present model, the leptonic CP-violation turns out to be similar to Refs. [36,110–113,127–135]. The moduli and phase of non-unitarity and CP-violating parameter for the degenerate case of the present models are

$$\begin{aligned}|\eta_{e\mu}| &= 2.73\times 10^{-8},\\ \delta_{e\mu} &= 1.920,\\ |\eta_{e\tau}| &= 4.54\times 10^{-7},\\ \delta_{e\tau} &= 1.78,\\ |\eta_{\mu\tau}| &= 2.31\times 10^{-5},\\ \delta_{\mu\tau} &= 2.39\times 10^{-7}.\end{aligned} \quad (47)$$

The estimations presented in Eq. (47) show that in a wider range of the parameter space, the leptonic CP violation parameter could be nearly two orders larger than the CKM-CP violation parameter for quarks.

6 Neutrino-less double beta decay

Even with the vanishing bare mass term $\mu_S = 0$ in the Yukawa Lagrangian of Eq. (10), the singlet fermions $S_i (i = 1, 2, 3)$ acquire Majorana masses over a wide range of values and, in the leading order, the corresponding mass matrix given in Eq. (14) is $m_S = -M\frac{1}{M_N}M^T$. As far as the light-neutrino mass matrix is concerned, it is given by the Type-II seesaw formula of Eq. (20), which is independent of the Majorana mass matrix m_S of singlet fermions. But the combined effect of substantial mixing between the light neutrinos and the singlet or the RH neutrinos and also between the singlet neutrinos and the RH neutrinos result in the new Majorana neutrino mass insertion terms in the Feynman diagrams. Out of these the mass insertion m_S due to the singlet fermions in the Feynman diagram gives rise to new dominant contributions to the amplitude and the effective mass parameter for $0\nu\beta\beta$ even in the W_L–W_L channel. This may be contrasted with the conventional Type-II seesaw dominated non-SUSY SO(10) models with only three generations of standard fermions in $\mathbf{16_i}(i = 1, 2, 3)$, where there are no such contributions to $0\nu\beta\beta$ decay. The generalised form of the charged current interaction Lagrangian for leptons in this model including both $V \pm A$ currents has been given in Eq. (37).

As stated above, in Model I and Model II, the $W_R^{\pm}$ bosons and the doubly charged Higgs scalars, both the left-handed and the right-handed, are quite heavy with $M_{W_R} \sim M_\Delta \simeq 10^8$–$10^9$ GeV. These make negligible contributions due to the RH current effects and Higgs exchange effects for the $0\nu\beta\beta$ decay amplitude. The most popular standard and conventional contribution in the W_L^-–W_L^- channel is due to light neutrino exchanges. But one major new point in this work is that even in the W_L^-–W_L^- channel, the singlet fermion exchange, allowed within the Type-II seesaw dominance mechanism, can yield a much more dominant contribution to the $0\nu\beta\beta$ decay rate. For the exchange of singlet fermions $(\hat{S}_j)$, the Feynman diagram is shown in Fig. 5. For the exchange of heavier RH Majorana neutrinos $(\hat{N}_k)$, the diagram is the same as this figure but with the replacement of the mixing matrix and masses by $\mathcal{V}^{\nu S} \to \mathcal{V}^{\nu N}$ and $m_{S_i} \to M_{N_i}$. The heavier RH neutrino exchange contributions are found to be negligible compared to the singlet fermion exchange contributions. In the mass basis, the contributions to the decay amplitudes by ν and S and N exchanges are estimated as

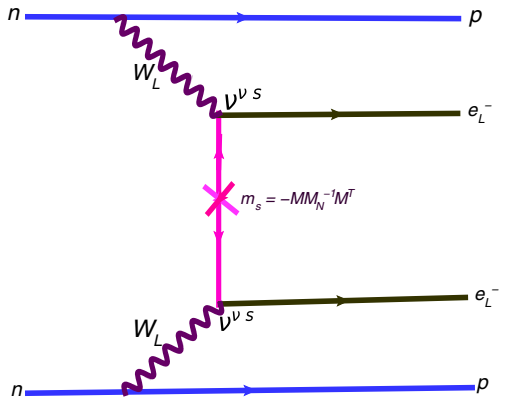

Fig. 5 Feynman diagrams for neutrino-less double beta decay contribution with virtual Majorana neutrinos $\hat{\nu}_i$ and $\hat{S}_i$ in the W_L–W_L-channel. For the RH neutrino exchange the Feynman diagram is the same but with the replacements $\mathcal{V}^{\nu S} \to \mathcal{V}^{\nu N}$, $S_i \to N_i$

$$\mathcal{A}_\nu^{LL} \propto \frac{1}{M_{W_L}^4} \sum_{i=1,2,3} \frac{\left(\mathcal{V}_{ei}^{\nu\nu}\right)^2 m_{\nu_i}}{p^2}, \tag{48}$$

$$\mathcal{A}_S^{LL} \propto \frac{1}{M_{W_L}^4} \sum_{j=1,2,3} \frac{\left(\mathcal{V}_{ej}^{\nu S}\right)^2}{m_{S_j}}, \tag{49}$$

$$\mathcal{A}_N^{LL} \propto \frac{1}{M_{W_L}^4} \sum_{j=1,2,3} \frac{\left(\mathcal{V}_{ej}^{\nu N}\right)^2}{m_{N_j}}, \tag{50}$$

where $|p| \simeq 190$ MeV represents the magnitude of the neutrino virtuality momentum [136–146]. Using the uncertainties in the nuclear matrix elements [144–147] we have found it to have values in the range $|p| = 120$–200 MeV.

7 Effective mass parameter and half-life

Adding together the $0\nu\beta\beta$ decay amplitudes arising out of light neutrino exchanges, singlet fermion exchanges and the heavy RH neutrino exchanges in the W_L–W_L channel from Eq. (49), and using suitable normalisations [144–147], we express the inverse half-life thus:

$$\begin{aligned}\left[T_{1/2}^{0\nu}\right]^{-1} &\simeq G_{01}^{0\nu} |\frac{\mathcal{M}_\nu^{0\nu}}{m_e}|^2 |(\mathbf{m}_\nu^{ee} + \mathbf{m}_S^{ee} + \mathbf{m}_N^{ee})|^2, \\ &= K_{0\nu} |(\mathbf{m}_\nu^{ee} + \mathbf{m}_S^{ee} + \mathbf{m}_N^{ee})|^2, \\ &= K_{0\nu} |\mathbf{m}_{\rm eff}|^2. \end{aligned} \tag{51}$$

In the above equation $G_{01}^{0\nu} = 0.686 \times 10^{-14}\text{years}^{-1}$, $\mathcal{M}_\nu^{0\nu} = 2.58 - 6.64$, $K_{0\nu} = 1.57 \times 10^{-25}\text{years}^{-1}\text{eV}^{-2}$ and the three effective mass parameters for light neutrino, singlet fermion and heavy RH neutrino exchanges are

$$\mathbf{m}_\nu^{\rm ee} = \sum_i \left(\mathcal{V}_{ei}^{\nu\,\nu}\right)^2 m_{\nu_i}, \tag{52}$$

$$\mathbf{m}_S^{\rm ee} = \sum_i \left(\mathcal{V}_{ei}^{\nu S}\right)^2 \frac{|p|^2}{m_{S_i}}, \tag{53}$$

$$\mathbf{m}_N^{\rm ee} = \sum_i \left(\mathcal{V}_{ei}^{\nu N}\right)^2 \frac{|p|^2}{m_{N_i}}, \tag{54}$$

with

$$\mathbf{m}_{\rm eff} = \mathbf{m}_\nu^{ee} + \mathbf{m}_S^{ee} + \mathbf{m}_N^{ee}. \tag{55}$$

Here m_{S_i} is the eigenvalue of the S-fermion mass matrix m_S, and the magnitude of neutrino virtuality momentum $|p| = 120$–200 MeV. As the predicted values of the RH neutrino masses carried out in Sect. 3 have been found to be large, which makes their contribution to the $0\nu\beta\beta$ decay amplitude negligible, we retain only contributions due to light neutrino and singlet fermion exchanges. The estimated values of the effective mass parameters due to the S-fermion exchanges and light neutrino exchanges are shown separately in Fig. 6 where the magnitudes of the corresponding mass eigenvalues used have also been indicated.

7.1 Numerical estimations of effective mass parameters

Using the equations of the normalised mass parameters [37], we estimate numerically the nearly standard contribution due to the light neutrino exchanges and the dominant non-standard contributions due to the singlet fermion exchanges.

7.1.1 A. Nearly standard contribution

In this model the new mixing matrix $\mathcal{N} \equiv \mathcal{V}^{\nu\nu} = (1-\eta)\, U_\nu$ contains an additional non-unitarity effect due to the non-vanishing η [37]. Using $M_{\rm Deg} = 1213$ GeV in the degenerate case, we estimate

$$\mathcal{N}_{ei} = (0.81437,\ 0.54858,\ 0.1267 + 0.0922i). \tag{56}$$

Since all the η-parameters are constrained by $|\eta_{\alpha\beta}| < 10^{-3}$, it is expected that $|\mathcal{N}_{ei}| \simeq |U_{ei}|$ for any other choice of M. In the leading approximation, by neglecting the $\eta_{\alpha i}$ contributions, the effective mass parameter in the W_L–W_L channel with light neutrino exchanges is expressed as

$$\begin{aligned} m_\nu^{\rm ee} &= \sum_i \mathcal{N}_{ei}^2 \hat{m}_i \\ &\simeq (c_{12}c_{13})^2 \hat{m}_1 e^{i\alpha_1} + (s_{12}c_{13})^2 \hat{m}_2 e^{i\alpha_2} \\ &\quad + s_{13}^2 e^{i\delta} \hat{m}_3, \end{aligned} \tag{57}$$

where we have introduced the two Majorana phases α_1 and α_2. As discussed subsequently in this section, they play crucial roles in preventing the cancellation between two different effective mass parameters. Using $\alpha_1 = \alpha_2 = 0$ and the

experimental values of light-neutrino masses and the Dirac phase $\delta = 0.8\pi$ from Eq. (21), the light neutrino exchanges have their well known values,

$$|m_\nu^{\rm ee}| = \begin{cases} 0.0039\,{\rm eV} & {\rm NH}, \\ 0.04805\,{\rm eV} & {\rm IH}, \\ 0.23\,{\rm eV} & {\rm QD}. \end{cases} \quad (58)$$

7.1.2 B. Dominant non-standard contributions

The (ei) element of the ν–S mixing matrix is [37]

$$\mathcal{V}_{ei}^{\nu S} = \left(\frac{M_D}{M}\right)_{ei}, \quad (59)$$

where the Dirac neutrino mass matrix M_D has been given in Eq. (36), and the diagonal elements are estimated using the non-unitarity equation as discussed in the previous section. We derive the relevant elements of the mixing matrix $\mathcal{V}^{\nu S}$ using the structures of the Dirac neutrino mass matrix M_D given in Eq. (36) and values of the diagonal elements of $M = (M_1, M_2, M_3)$ satisfying the non-unitarity constraint in Eq. (43). The eigenvalues of the S-fermion mass matrix m_S are estimated for different cases using the structures of the RH Majorana neutrino mass matrices given in Eqs. (26), (28) and (30) in the formula $m_S = -M\frac{1}{M_N}M^T$. It is clear that in the effective mass parameter the non-standard contribution due to sterile fermion exchange has a sign opposite to that due to light neutrino exchange, and also its magnitude is inversely proportional to the sterile fermion mass eigenvalues. In the NH case the estimated effective mass parameters are shown in Fig. 6 where the values of the diagonal elements of M and the eigenvalues of m_s have been specified.

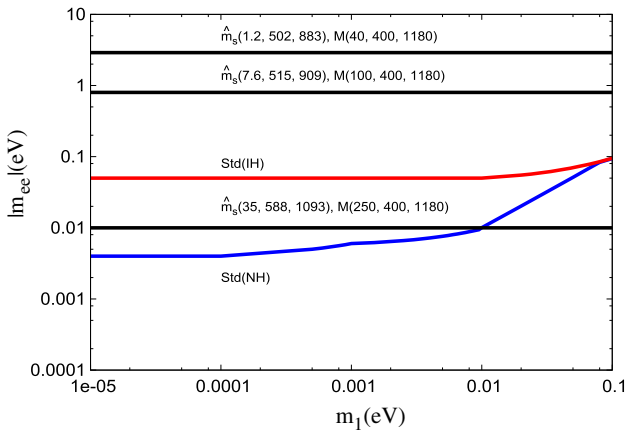

Fig. 6 Variation of the effective mass parameters with lightest LH neutrino mass. The dominant non-standard contributions due to fermion singlet contributions are shown by three horizontal lines with corresponding mass values in GeV units. The subdominant effective mass parameters due to the NH and IH cases shown are similar to the standard values

For comparison, the effective mass parameters in the standard case without singlet fermions have been also given. It is clear that for allowed masses of the model, the non-standard contributions to the effective mass parameters can be much more dominant compared to the standard values irrespective of the mass patterns of the light-neutrino masses: NH, IH, or QD.

7.2 Cancellation between effective mass parameters

When plotted as a function of singlet fermion mass eigenvalue m_{S_1}, the resultant effective mass parameter shows a cancellation for a certain region of the parameter space, the cancellation being prominent in the QD case. Like the light-neutrino masses, the singlet fermion masses m_{S_i} are also expected to have two Majorana phases. When all Majorana phases are absent, both in the light active neutrino as well as in the singlet fermion sectors, it is clear that in the sum of the two effective mass parameters there will be a cancellation between the light active neutrino and the singlet fermion contributions because of the inherent negative sign of the non-standard contribution. Our estimations for the NH, IH and QD patterns of light-neutrino mass hierarchies are discussed separately.

7.2.1 A. Effective mass parameter for NH and IH active neutrino masses

In Fig. 7, we show the variation of the resultant effective mass parameter with m_{S_1} for NH and IH patterns of active light-neutrino masses. It is clear that for lower values of m_{S_1}, the singlet fermion exchange term continues to dominate. For larger values of m_{S_1} the resultant effective mass parameter tends to be identical to the light-neutrino mass contribution due to the vanishing non-standard contribution. We note that

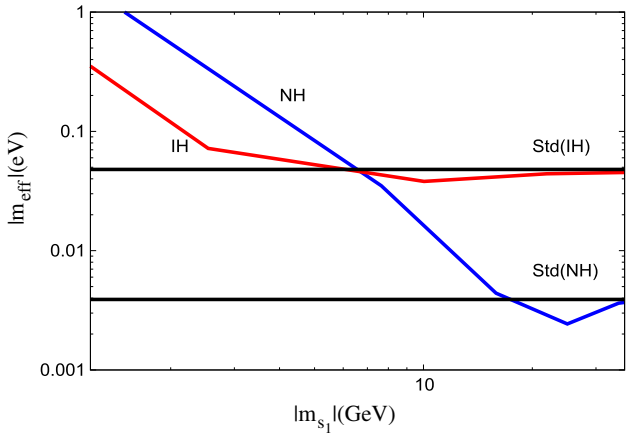

Fig. 7 Variation of effective mass parameter of $0\nu\beta\beta$ decay with the mass of the lightest singlet fermion for $|p| = 190$ MeV

the values $|m_{\rm eff}| = 0.5$–0.1 eV can easily be realised for $|m_{S_1}| = 3$–5 GeV in the NH case but for $|m_{S_1}| = 1$–2 GeV in the IH case.

7.2.2 B. Effective mass parameter for QD neutrinos

The variation of the effective mass with m_{S_1} for the QD case with one experimentally determined Dirac phase $\delta = 0.8\pi$ and assumed values of two unknown Majorana phases is given in Fig. 8. The upper panel of Fig. 8 shows the variation with $\alpha_1 = \alpha_2 = 0$ for different choices of the common light-neutrino mass $m_0 = 0.5$ eV, 0.3 eV and 0.2 eV for the upper, middle and the lower curves, respectively, where the cancellations are clearly displayed in the regions of $m_{s_1} = 0.4$–1.5 GeV. However, before such a cancellation occurs, the dominance of the singlet exchange contribution is clearly shown to occur in the regions of lower values of m_{S_1}. For larger values of $m_{S_1} > 5$ GeV, the singlet exchange contribution tends to be negligible and the light QD neutrino contribution to $m_{\rm eff}$ is recovered. In the lower panel of Fig. 8, the upper curve corresponds to $\alpha_1 = \pi$, $\alpha_2 = \pi$ at $m_0 = 0.2$ eV. The middle line corresponds to $\alpha_1 = \pi$, $\alpha_2 = 0$ at $m_0 = 0.5$ eV. The lower line corresponds to $\alpha_1 = 0$, $\alpha_2 = \pi$ at $m_0 = 0.3$ eV. We find that because of the introduction of the appropriate Majorana phases the dips in the two curves have disappeared.

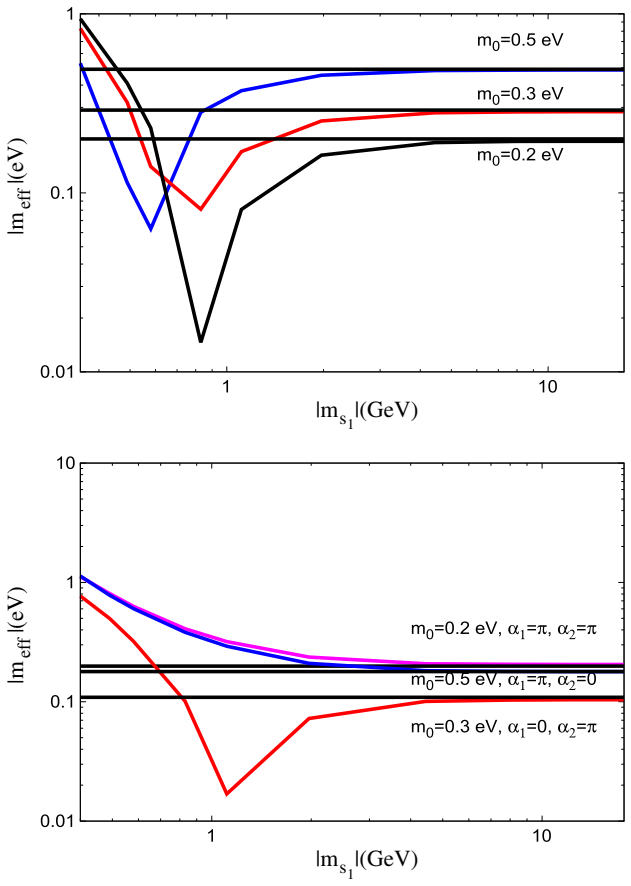

Fig. 8 Variation of the effective mass of $0\nu\beta\beta$ decay with the mass of the lightest singlet fermion for QD light neutrinos with one Dirac phase (*upper*) and with one Dirac phase and two Majorana phases (*lower*)

7.3 Half-life as a function of singlet fermion masses

In order to arrive at a plot of the half-life against the lightest singlet fermion mass in different cases, at first we estimate the mass eigenvalues of the three singlet fermions for different allowed combinations of the N–S mixing matrix elements satisfying the non-unitarity constraint of Eq. (43) and by using the RH neutrino mass matrices predicted for the NH, IH and QD cases from Eqs. (26), (28), (30) and (31). These solutions are shown in Table 4.

We then derive expressions for the half-life taking into account the contributions of the two different amplitudes or effective mass parameters arising out of the light neutrino and the singlet fermion exchanges, leading to

$$\left[T^{0\nu}_{1/2}\right] = \frac{m_{s1}^2}{K_{0\nu}|p|^4 (M_D/M)_{e1}{}^4}\left[|1 + X + Y|\right]^{-2}, \tag{60}$$

where

$$X = \frac{(M_D/M)_{e2}{}^2}{(M_D/M)_{e1}{}^2}\frac{m_{S_1}}{m_{s_2}} + \frac{(M_D/M)_{e3}{}^2}{(M_D/M)_{e1}{}^2}\frac{m_{S_1}}{m_{S_3}}, \tag{61}$$

$$Y = \mathbf{m}_\nu^{ee}\frac{m_{S_1}}{p^2 (M_D/M)_{e1}^2}. \tag{62}$$

Here we have used the expression for $\mathbf{m}_\nu^{ee}$ given in Eq. (52). In Eq. (60), $Y = 0$ gives complete dominance of the singlet fermion exchange term. However, this formula for the half-life is completely different from the one obtained using inverse seesaw dominance in SO(10) [39]. In the present model in the leading order, the predicted half-life depends directly on the square of the lightest singlet fermion mass and it is independent of the RH neutrino mass, which is non-diagonal. But in [39], the half-life of neutrino-less double beta decay is directly proportional to the fourth power of the lightest singlet fermion mass and the square of the lightest right-handed neutrino mass, leading to a different result.

7.3.1 A. Half-life in the NH and IH cases

We have computed the half-life for NH and IH patterns of active neutrino masses, taking the contributions of singlet fermion as well as light active neutrino exchanges. This is shown in the upper panel for the NH case and in the lower panel for the IH case in Fig. 9.

Taking both the X term and the Y term in Eq. (60), we find that for a smaller value of m_{S_1}, the contribution due

Table 4 Eigenvalues of singlet fermion masses for different allowed N–S mixing matrix elements and for NH, IH and QD patterns of light-neutrino masses

M (GeV)	$\hat{m_s}(NH)$ (GeV)	M (GeV)	$\hat{m_s}(IH)$ (GeV)	M (GeV)	$\hat{m_s}(QD)$ (GeV)
(40,400,1180)	(1.2,502,883)	(40,450,1280)	(0.4,54.32,7702)	(100,600,1500)	(0.5,17.7,109))
(100,400,1180)	(7.65,515,909))	(60,450,1280)	(0.9,54.4,7705)	(130,600,1500)	(0.8,17.7,109)
(150,400,1180)	(16,533,951)	(70,450,1280)	(1.2,54.4,7706)	(200,600,1500)	(1.97,17.7,109)
(200,400,1180)	(25,558,1011)	(100,450,1280)	(2.5,55,7715)	(300,600,1500)	(4.4,17.7,109)
(250,400,1180)	(35,588,1093)	(300,450,1280)	(22,56,7831)	(350,600,1500)	(6.05,17.7,109)
(300,400,1180)	(43,622,1200)	(400,450,1280)	(36.2,59,7933)	(400,600,1500)	(8,17.7,109)
(350,400,1180)	(50,659,1331)	(450,450,1280)	(42,64,7996)	(500,600,1500)	(12.3,17.7,109)
				(600,600,1500)	(17.7,17.7,109)

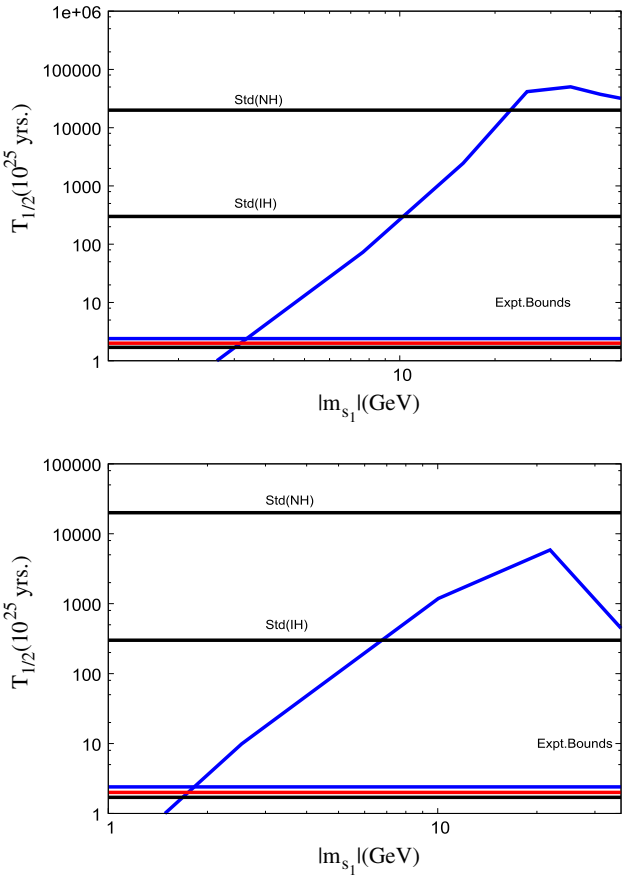

Fig. 9 Variation of half-life of $0\nu\beta\beta$ decay with the sterile neutrino mass for the NH (*upper*) and the IH (*lower*) patterns of the light active neutrino masses for $|p| = 190$ MeV

to the sterile neutrino is dominated for both the NH and the IH cases. But with the increase in the value of m_{S_1}, the half-life increases, showing its decreasing strength. The predicted half-life curve saturates the experimental data at $m_{S_1} \simeq 3\,\text{GeV}$ and $m_{S_1} \simeq 2\,\text{GeV}$ for the NH and the IH cases, respectively. The interesting predictions are that if the lightest sterile neutrino mass satisfies the bound $m_{S_1} \leq 3\,\text{GeV}$, then the $0\nu\beta\beta$ decay should be detected with half-life close to the current experimental bound even if the light-neutrino masses have the NH pattern of masses. Similarly the corresponding bound for the IH case is $m_{S_1} \leq 2\,\text{GeV}$. But in a recent paper [39] which has an inverse seesaw dominant neutrino mass, the corresponding bound for the NH and IH case is $m_{S_1} \leq 14\,\text{GeV}$.

7.3.2 B. Lifetime prediction with QD neutrino masses.

For the QD masses of the light active neutrinos, we considered the X term and Y term of Eq. (60) i.e. including both the sterile neutrino exchange and the light neutrino exchange contributions. For the light-neutrino effective mass parameter occurring in Y, we have considered three different cases with common light-neutrino mass values $m_0 = 0.2\text{eV}, 0.3\text{eV}$ and 0.5eV, resulting in the three different curves shown in the upper and the lower panels of Fig. 10. In the upper panel, only the experimentally determined Dirac phase $\delta = 0.8\pi$ has been included in the PMNS mixing matrix for light QD neutrinos, while ignoring the two Majorana phases ($\alpha_1 = \alpha_2 = 0$). In the lower panel, while keeping $\delta = 0.8\pi$ for all the three curves, the Majorana phases have been chosen as indicated against each of them. As the sterile neutrino exchange amplitude given in Eq. (53) is inversely proportional to the eigenvalue of the corresponding sterile neutrino mass m_{S_i}, even in the quasi-degenerate case this contribution is expected to dominate for allowed small values of m_{S_i}. This fact is reflected in both figures given in Fig. 10. When the Majorana phases are ignored, this dominance gives a half-life less than the current bounds for $m_{S_1} < 0.5\,\text{GeV}$ when $m_0 = 0.5$ eV, but for $m_{S_1} < 0.7$ GeV when $m_0 = 0.2$–0.3 eV. When the Majorana phases are included preventing cancellation between the two contributions, these crossing points are changed to $m_{S_1} < 0.7\,\text{GeV}$ when $m_0 = 0.3$ eV, but $m_{S_1} < 1.0\,\text{GeV}$ when $m_0 = 0.2$–0.5 eV. Repeating the same procedure as for Ref. [39] which is based upon inverse seesaw dominance, the corresponding bound for the QD case is $m_{S_1} \leq 12.5\,\text{GeV}$.

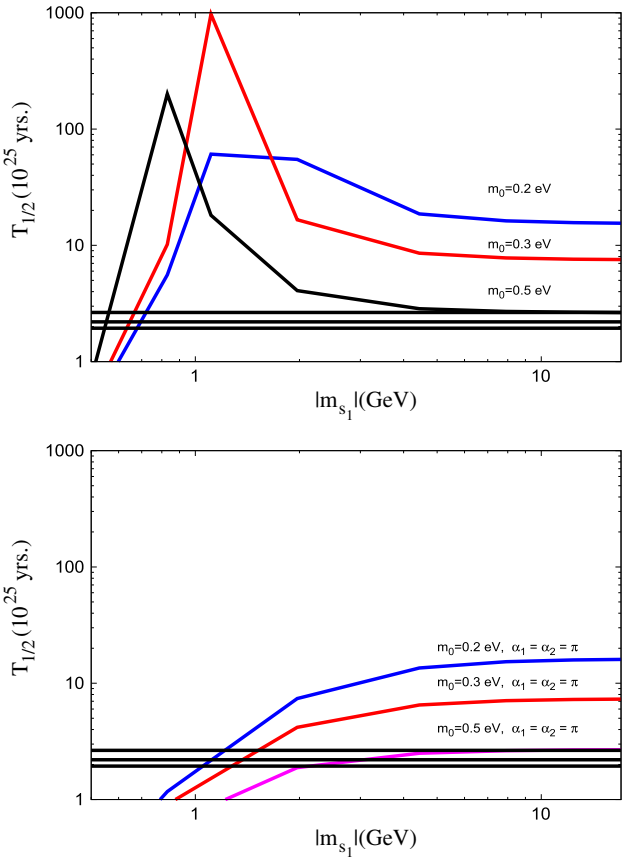

Fig. 10 Variation of half-life of $0\nu\beta\beta$ decay with the mass of the lightest singlet fermion for QD light neutrinos including one Dirac phase (*upper curve*) and one Dirac phase and two Majorana phases (*lower curve*)

In the present case, the peaks in the half-life prediction appear because of cancellation between the two effective parameters. The inclusion of the Majorana phases annuls the cancellation, resulting in the constructive addition of the two effective mass parameters and reduced values of the half-life accessible to ongoing searches. For larger values of $m_{S_1} >> 20\,\text{GeV}$, the sterile neutrino contribution to the $0\nu\beta\beta$ amplitude becomes negligible and the usual contributions due to light quasi-degenerate neutrinos are recovered.

8 Brief discussion of other aspects and leptogenesis

Here we discuss briefly constraints imposed on the model by electroweak precision observables and predictions on the order of magnitude of baryon asymmetry of the universe through resonant leptogenesis [148]. We also point out the occurrence of small Z–Z' mixings, while indicating briefly a possible application for dilepton production. Since details of analyses and predictions on these aspects are beyond the scope of this paper, they will be presented elsewhere [149].

8.1 Electroweak precision observables and other constraints

We have shown that dominant contributions to $0\nu\beta\beta$ decay are possible for the first generation sterile neutrino masses $\hat{m}_{S_1} \sim \mathcal{O}(1)\,\text{GeV}$. For larger values of this mass $\hat{m}_{S_1} \sim$ 5–10 GeV partial cancellation between the effective mass parameters due to light neutrino and sterile neutrino exchanges occurs depending upon the choices of different Majorana phases. Various lighter sterile mass eigenvalues relevant for $0\nu\beta\beta$ decay are shown in Table 4 in the NH, IH and QD cases. It is pertinent to discuss the influence of these lighter masses on the precision electroweak observables.

For the choices of parameters permitted by observable LFV and/or dominant LNV, the sterile fermion masses of the first two generations could be $\hat{m}_{s_i} < 45\,\text{GeV}$, $i = 1, 2$, whereas in the absence of dominant LNV decay, the mass eigenvalues could be even larger, $\hat{m}_{s_i} \simeq 500\,\text{GeV}$. When they are in the range of 1–45 GeV, we have estimated the corresponding corrections on the electroweak observables. The ν–S mixing $\mathcal{V}^{\nu S} = (\frac{M_D}{M})_{\nu S}$ is well determined in our model and all the relevant ν–S mixings are easily deduced using Eqs. (36) and (43). In the allowed kinematical region, we have estimated the partial decay widths,

$$\Gamma(Z \to S_i S_i) = \Gamma_Z^{\nu\bar{\nu}} \left[\sum_\alpha |\left(\mathcal{V}_{\alpha,i}^{\nu S}\right)|^4 \right] (i = 1, 2), \qquad (63)$$

where the standard value $\Gamma_Z^{\nu\bar{\nu}} = 0.17\,\text{GeV}$ and $\mathcal{V}_{\alpha,i}^{\nu S} = (M_D/M)_{\alpha,i}$ with $\alpha = \nu_e, \nu_\mu, \nu_\tau$ and $i = 1, 2, 3$. We then obtain $\Gamma(Z \to S_1 S_1) = 1.2 \times 10^{-14}\,\text{GeV}$ for the NH, IH and QD cases, and $\Gamma(Z \to S_2 S_2) = 6.6 \times 10^{-11}\,\text{GeV}$ for the QD case only. Similarly we have estimated the partial decay width

$$\Gamma(W \to l S_i) = \Gamma_W^{l\nu} \left[\sum_\alpha |\left(\mathcal{V}_{\alpha,i}^{\nu S}\right)|^2 \right] (i = 1, 2), \qquad (64)$$

and we obtained $\Gamma(W \to e S_1) \simeq \Gamma(W \to e S_2) = 3.5 \times 10^{-9}\,\text{GeV}$, $\Gamma(W \to \mu S_1) \simeq \Gamma(W \to \mu S_2) = 1.8 \times 10^{-7}\,\text{GeV}$ and $\Gamma(W \to \tau S_1) \simeq \Gamma(W \to \tau S_2) = 1.0 \times 10^{-5}\,\text{GeV}$. These and other related estimations cause negligible effects on the electroweak precision observables [150] primarily because of the small ν–S mixings determined by the model analyses. In addition to these insignificant tree level corrections, new physics effects may affect the electroweak observables indirectly via oblique corrections through loops' leading corrections to the Peskin–Takeuchi S, T, U parameters [151–153]. Although the computation of these loop effects are beyond the scope of the present paper, it may be interesting to estimate how the new fermions through their small mixings with active neutrinos may affect the lep-

tonic and the invisible decay widths of the Z-boson, the W-mass and other observables [149].

In this model the neutral generator corresponding to heavy Z' is a linear combination of the $U(1)_R$ and $U(1)_{B-L}$ generators, while the other orthogonal combination is the $U(1)_Y$ generator of the SM (for earlier work on, Z' boson in GUTs embedding two-step breaking of left-right gauge symmetry, see [33–35]), [66–68]. The Z–Z' mixing in such theories is computed through the generalised formula $\tan^2\theta_{zz'} = \frac{M_0^2-M_Z^2}{M_{Z'}^2-M_0^2}$ where $M_0 = \frac{M_W}{\sqrt{\rho_0}\cos\theta_W}$. In our model, since the LH triplet $\Delta_L(3,-1,1)$ has a very small VEV, $v_L = 0.1$–0.5 eV $<< V_{\rm ew}$, the model is consistent with the tree level value $\rho_0 = 1$. The radiative corrections due to the 125 GeV Higgs of the SM and the top quark yield $\rho \simeq 1.009$ [154]. The new neutral gauge boson Z' in principle may have an additional influence on the electroweak precision parameters as well as the Z-pole parameters if $M_{Z'} << \mathcal{O}(1)$ TeV [66–68,155–157]. The most recent LHC data has given the lower bound $M_{Z'} \geq 1.6$ TeV [158–160]. Since our model is based on an extended seesaw mechanism, we require $V_R >> V_{ew} = 246$ GeV and this implies $M_{Z'} >> M_Z$ but accessible to LHC. Under this constraint $M_{Z'} \sim \mathcal{O}(5$–$10)$ TeV are the most suitable predictions of both models discussed in this work. As some examples, using such values of $M_{Z'}$ and the reported values from the Particle Data Group [161–163] of $\sin^2\theta_W = 0.23126 \pm 0.00005$, $M_W = 80.385 \pm 0.015$GeV, $M_Z = 91.1876 \pm 0.0021$ GeV, $\rho_0 = 1.01$, we obtain $\theta_{zz'} = 0.00131 \pm 0.0003$, 0.0005 ± 0.00012, 0.0003 ± 0.00008 and 0.0002 ± 0.00006 for $M_{Z'} = 2.0$TeV, 5.0TeV, 7.5TeV and 10TeV, respectively. Because of the smallness of the values, these mixings are consistent with the electroweak precision observables including the Z-pole data [66–68,155–157,164,165]. Some of these masses may also be in the accessible range of the ILC [166]. Details of the experimental constraints on Z–Z' mixings as a function of the Z' masses will be investigated elsewhere [149].

8.2 Possibility of dilepton signals at LHC

In both models considered in this work, there are two types of heavy Majorana neutrinos: (i) the RH neutrinos with masses $M_{N_i} \geq \mathcal{O}(1$–$10)$ TeV, (ii) some of the three sterile neutrinos with masses $\hat{m}_{S-i} << M_{N_i}$. In principle both of these classes of fermions are capable of contributing to dilepton production at LHC through the sub-processes $pp \to W_L^{\pm} \to l^{\pm}l^{\pm}jjX$ where, for example, the W_L^+ produced from pp collision gives rise to a charged lepton l^+ and a N_i or S_i in the first step by virtue of the latter's mixing with the charged leptons given in Eq. (39). The particle N_i or S_i can then produce a second charged lepton of the same sign and a W_L^- boson that is capable of giving rise to two jets. It is interesting to note that our model predicts a rich structure of like sign dilepton production through the mediation of N_i or S_i, or both. From the details of the model parametrisations discussed in Sects. 3–5, we have found the corresponding mixing matrices with charged leptons defined through Eq. (39) discussed in Sect. 5. We have estimated the elements $\mathcal{V}_{e1}^{\nu N} \simeq -0.0000727 + i0.000203$ and $\mathcal{V}_{\mu 2}^{\nu N} \simeq 0.000813 - i0.001148$, which would contribute to the production cross sections of $pp \to e^{\pm}e^{\pm}jjX$ and $pp \to \mu^{\pm}\mu^{\pm}jjX$ by the exchange of RH neutrinos, the cross sections being proportional to the modulus squares of these mixings. Similarly, we have $\mathcal{V}_{\mu 2}^{\nu S} \simeq 0.0003191$, which can also contribute to production process $pp \to \mu^{\pm}\mu^{\pm}jjX$ by the exchange of the second sterile neutrino mass eigenstate. The first sterile neutrino is too light to mediate the dilepton production process detectable inside the LHC detector itself. Thus the LHC evidence of dilepton production signals may indicate the presence of heavy Majorana neutrinos (see, for instance [109]). Details of the predictions will be reported elsewhere [149].

8.3 Leptogenesis

This model may have a wider range of possibilities for leptogenesis via decays of Higgs triplets [167], or through the decays of LHC scale Majorana fermions N or S. Although a rigorous estimation including solutions of the Boltzmann equations is beyond the scope of this work (it will be addressed elsewhere [149]), we discuss here briefly only a plausible case with a very approximate estimation of the CP-asymmetry parameter and the order of magnitude of the baryon asymmetry through the decays of two nearly degenerate Majorana masses of sterile neutrinos. For resonant leptogenesis through the decays of a pair of quasi-degenerate RH neutrinos, relevant formulas for CP-asymmetry and baryon asymmetry have been suggested in [148]. Noting that $\hat{m}_{S_1} \sim \mathcal{O}(1)$ GeV is important for a dominant contribution to $0\nu\beta\beta$ decay and the N–S mixing matrix elements $M_2 \sim M_3 \simeq \mathcal{O}(1)$ TeV are capable of predicting experimentally accessible LFV decays in our model, we choose an interesting region of the parameter space $M \simeq$ diag.$(146, 3500, 3500)$ GeV in the quasi-degenerate case of S_2 and S_3. Then, using the G_{2113} breaking VEV $V_R \simeq \mathcal{O}(10)$ TeV, the results of Sect. 3.3 in the QD case of active neutrinos and Eq. (14), we obtain

$$\hat{m}_{S_i} = \text{diag.}(1.0, 595.864..., 595.864...)\text{GeV}, \tag{65}$$

where the ellipses on the RHS indicate higher degrees of quasi-degeneracy of the two masses the model tolerates. In order to estimate lepton asymmetry caused by the decay of

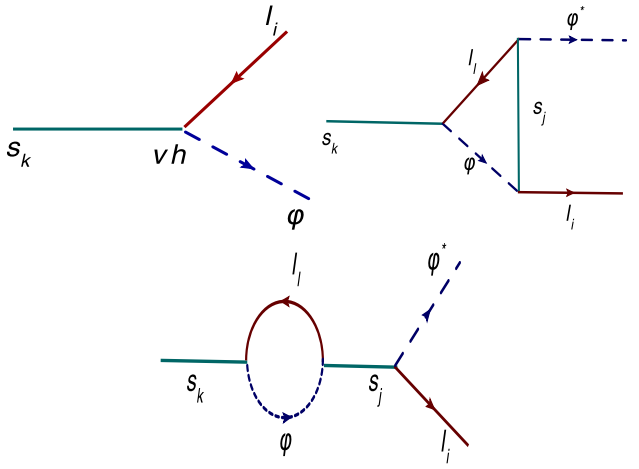

Fig. 11 Tree and one-loop diagrams for the S_k decay contributing to the CP-asymmetry. All fermion–Higgs couplings in the diagrams are of the form Vh where we have the $h = N$–l–Φ Yukawa coupling and $V \simeq M/M_N$

heavy sterile fermions $\hat{S}_k (k = 2, 3)$ via their mixing with the heavier RH neutrinos, the corresponding Feynman diagrams at the tree and one-loop levels, including the vertex and self-energy diagrams, are shown in Fig. 11.

The fermion–Higgs coupling in all the diagrams is Vh instead of the standard Higgs-Yukawa coupling $h = M_D/V_{\rm wk}$, where $\mathcal{V} \simeq M/M_N$, M_D is given in Eq. (36) and $V_{\rm wk} \simeq 174\,{\rm GeV}$. The widths of these sterile fermions are $\Gamma_{S_2} \simeq 16.3$ keV and $\Gamma_{S_3} \simeq 14.0$ MeV. In order to exploit the quasi-degeneracy of the second and the third generation fermions in resonant leptogenesis, we use the formula for CP-asymmetry generated due to interference between the tree and the self-energy graphs [148],

$$\varepsilon_{S_k} = \sum_j \frac{\mathcal{I}m[(y^\dagger y)^2_{kj}]}{|y^\dagger y|_{jj}|y^\dagger y|_{kk}} R$$
$$R = \frac{(\hat{m}^2_{S_i} - \hat{m}^2_{S_j})\hat{m}_{S_i}\Gamma_{S_j}}{(\hat{m}^2_{S_i} - \hat{m}^2_{S_j})^2 + \hat{m}^2_{S_i}\Gamma^2_{S_j}}, \tag{66}$$

where $y = M/M_N h$, $h = M_D/V_{\rm wk}$ and $V_{\rm wk} \simeq 174$ GeV. For a computation of the baryon asymmetry Y_B with a given wash-out factor K, we have also utilised the formula suggested in Ref. [148]:

$$Y_B \simeq \frac{\varepsilon_{S_k}}{200 K_k},$$
$$K_k = \frac{\Gamma_{S_k}}{H(\hat{m}_{S_k})}, \tag{67}$$

$H(\hat{m}_{S_k})$ being the Hubble parameter at temperature $\hat{m}_{S_k}$. As in TeV scale leptogenesis models, here also we encounter large wash-out factors, which, in some cases, tend to damp out the baryon asymmetry generation. However, it has been shown [168] that all the $\Delta L = 2$ processes $l\Phi \to \bar{l}\Phi^\dagger$, expected to cause the most dominant wash-outs, are substantially depleted for the heavier quasi-degenerate Majorana masses of the decaying fermions. The depletion factor is proportional to δ_i^2 leading to an effective wash-out factor $K_i^{\rm eff}$, which replaces K_i for the ith decaying Majorana fermion,

$$\delta_i = \frac{|\hat{m}_{S_i} - \hat{m}_{S_j}|}{\Gamma_{S_i}} (i \neq j),$$
$$K_i^{\rm eff} \simeq \delta_i^2 K_i. \tag{68}$$

We find a sizeable baryon asymmetry in the following two cases: (i) In the case of finite perturbation theory, the $\hat{m}^2_{S_j}\Gamma^2_{S_j}$ term in the denominator of R has been noted to be absent [148] leading to a singular term in the CP-asymmetry. (ii) In the limit when $|\hat{m}_{S_i} - \hat{m}_{S_j}| << \Gamma_{S_j}/2$, $R = 2\frac{(\hat{m}_{S_i} - \hat{m}_{S_j})}{\Gamma_{S_j}}$.

(i) In finite perturbation theory

$$R = \frac{1}{2}\frac{\Gamma_j}{(\hat{m}_{S_j} - \hat{m}_{S_k})},$$
$$\delta_{jk} = \left(1 - \frac{\hat{m}_{S_j}}{\hat{m}_{S_k}}\right),$$
$$\varepsilon_{S_k} = \sum_j \frac{\mathcal{I}m[(y^\dagger y)^2_{kj}]}{16\pi |y^\dagger y|_{kk}\delta_{jk}}. \tag{69}$$

Similar formulas have been used by a number of authors in the case of decays of quasi-degenerate RH neutrinos [169] and, specifically, in the context of SO(10) [170]. For the decay of S_2 for which $K_2 = 2.7 \times 10^7$, using $(\hat{m}_{S_2} - \hat{m}_{S_3}) \simeq 2 \times 10^{-7}\,{\rm GeV}$, we obtain

$$\varepsilon_{S_2} = 0.824,$$
$$Y_B = 1.5 \times 10^{-10}. \tag{70}$$

The fine tuning in the quasi-degenerate masses can be reduced by one order if we use the effective wash-out factor. For example using $(\hat{m}_{S_2} - \hat{m}_{S_3}) \simeq 1.35 \times 10^{-6}\,{\rm GeV}$, we get $\delta_2 = 0.008$, leading to

$$\varepsilon_{S_2} = 0.0357,$$
$$K_2^{\rm eff} = 1.92 \times 10^5,$$
$$Y_B = 9.3 \times 10^{-10}. \tag{71}$$

For the decay of S_3 for which $K_3 = 2.4 \times 10^{10}$, using $(\hat{m}_{S_2} - \hat{m}_{S_3}) \simeq 10^{-6}\,{\rm GeV}$, we obtain $\delta_3^2 \simeq 5 \times 10^{-8}$, leading to

$$\varepsilon_{S_3} = 8 \times 10^{-5},$$
$$K_3^{\rm eff} = 575.4, \tag{72}$$
$$Y_B = 7.3 \times 10^{-10}.$$

(ii) In the larger width limit. $\Gamma_k > 2|(\hat{m}_{S_k} - \hat{m}_{S_j})|$,

$$R \simeq \frac{2(\hat{m}_{S_k} - \hat{m}_{S_j})}{\Gamma_k} \times \left[1 + \frac{4(\hat{m}_{S_k} - \hat{m}_{S_j})^2}{\Gamma_k^2}\right]^{-1},$$
$$\varepsilon_{S_k} = \sum_j \frac{\mathcal{I}m[(y^\dagger y)^2_{kj}]}{8\pi |y^\dagger y|_{kk} \Gamma_k} \hat{m}_{S_k} R. \quad (73)$$

This case can be more efficiently implemented for S_3 decay, which has $\Gamma_{S_3} \simeq 14$ MeV and $K_3 = 2.4 \times 10^{11}$. In this case the depletion in K_3 is quite effective. Using $(\hat{m}_{S_2} - \hat{m}_{S_3}) \simeq 10^{-6}$ GeV, we obtain $\delta_3^2 \simeq 5 \times 10^{-11}$, leading to

$$\varepsilon_{S_3} = 3 \times 10^{-7}, \quad K_3^{\text{eff}} = 10.3, \quad Y_B = 1.1 \times 10^{-10}. \quad (74)$$

Thus we have shown very approximately that the model may be capable of accommodating the order of magnitude of baryon asymmetry of the universe that requires fine tuning of the mass difference of the two sterile neutrino in the range 10^{-6}–10^{-7} GeV. In a separate paper we plan to look into an improvement in these approximate solutions and other possible channels of leptogenesis including the impact of the present model on electroweak precision observables and detection possibilities of RH neutrinos, S-fermions and the Z' at collider energies such as those of LHC and ILC [149].

9 Summary and conclusion

In this work we have investigated the prospect of having a new Type-II seesaw dominated neutrino mass generation mechanism in non-SUSY SO(10) GUT by a novel procedure by introducing one additional singlet fermion per generation. Following the popular view that the only meaningful fermion masses in the Lagrangian must have dynamical origins, and taking the non-dynamical singlet fermion mass μ_S to be negligible, one of the models (Model I) discussed is found to exhibit Type-II seesaw dominance and it predicts a TeV scale Z' boson accessible to LHC without any drastic fine tuning in the corresponding Yukawa sector. For Model II the desired Type-II seesaw dominance requires an additional fine tuning up to one part in a million. The would-be dominant Type-I seesaw contribution to neutrino masses in both models cancels out. The induced contribution to the ν–S mixing mass term M_L is shown to be damped out because of the GUT-scale mass of the LH doublet in 16_H, which renders the linear seesaw contribution to light neutrino masses naturally negligible in Model I, although in Model II it needs additional fine tuning. In spite of the high values of the Type-II seesaw scale $M_{\Delta_L} \simeq 10^8$–10^9 GeV $>> M_Z$, the models predict new dominant contributions to $0\nu\beta\beta$ decay in the W_L–W_L channel mediated by sterile neutrinos which acquire Majorana masses. The predicted LFV decay branching ratios for $\mu \to e\gamma$, $\tau \to \mu\gamma$ and $\tau \to e\gamma$, are found to be accessible to ongoing and planned experiments. We discuss the impact on the resultant effective mass parameter and the $0\nu\beta\beta$ half-life, showing the cancellation between light-neutrino exchange and sterile neutrino exchange contributions. The cancellation occurs because of the opposite signatures of the two effective mass parameters due to light neutrino exchange and the sterile neutrino exchange when the effects of the Majorana phases are ignored. We derive an analytic formula for the half-life of $0\nu\beta\beta$ decay as a function of the singlet fermion masses, predicting a lower bound on the lightest sterile neutrino mass eigenvalue from the current experimental data on the lower bounds. We find that the half-life close to the current lower bound or even lower can be easily accommodated even with the NH or IH patterns of light-neutrino masses. We find that the QD nature of the light-neutrino masses is not a necessary criterion to satisfy as regards existing lower bounds on the half-life estimated by different experimental groups. Even if the light active neutrino masses are NH or IH, a half-life prediction $T_{1/2} \simeq (2-5) \times 10^{25}$ years is realisable if the lightest sterile neutrino mass $m_{S_1} \simeq 2$–3 GeV. Depending upon the common mass of the light QD neutrinos, the model also predicts a lifetime $T_{1/2} \leq 2 \times 10^{25}$ years for $m_{S_1} \leq (0.5$–$1.0)$ GeV. A large cancellation between the two contributions is found to occur in the quasi-degenerate case of the light active neutrinos in the regions of a sterile neutrino mass, $m_{S_1} \simeq 2$–8 GeV. The bounds obtained in the sterile neutrino mass in these Type-II seesaw dominant models are significantly smaller than the bounds obtained in the inverse seesaw model [39]. As the sterile neutrino contribution to the $0\nu2\beta$ decay is inversely proportional to the corresponding mass eigenvalues, the smallness of the lightest mass eigenvalues causes dominant contributions compared to those by light neutrinos in NH, IH and QD cases. For the same reason the new contributions are damped out for large sterile neutrino mass eigenvalues. Because of the underlying Type-II seesaw formula for neutrino masses, heavy RH neutrino masses in the range $\mathcal{O}(100)$ GeV–$\mathcal{O}(10000)$ GeV and with specified heavy-light neutrino mixings are also predicted, which can be testified at the LHC and future high energy accelerators. The proton lifetime predictions for $p \to e^+\pi^0$ for some regions of the parameter space are also accessible to ongoing experimental searches, especially for intermediate mass values of the colour octet scalar which has been found to be necessary for gauge coupling unification. Further we have verified that the lighter S_1 or S_2 states in the models have

negligible effects on the values of the electroweak precision observables at the tree level although loop effects through the Peskin–Takeuchi parameters S, T, U will be investigated elsewhere. Approximate estimations show the occurrence of small Z–Z' mixings, apparently consistent with Z-pole and non-Z-pole data. The possibility of dilepton signals at LHC in the W_L–W_L channel is briefly noted in both models, while an approximate estimation indicates the possibility of baryon asymmetry generation through leptogenesis due to the decay of quasi-degenerate sterile Majorana fermions at the TeV scale. The details and rigorous estimations on dilepton signals, leptogenesis, estimation of S, T, U parameters and the impact of Z–Z' mixings on the Z-pole and non-Z-pole data including electroweak precision observables are currently under investigation and will be reported separately [149].

Acknowledgments M. K. P. thanks Thomas Hambye for discussion and the Department of Science and Technology, Govt. of India, for the research project, SB/S2/HEP-011/2013. B. N. thanks Siksha 'O' Anusandhan University for a research fellowship.

10 Appendix A

10.1 Beta function coefficients for RG evolution of gauge couplings

The RGEs for gauge couplings are

$$\mu\frac{\partial g_i}{\partial \mu} = \frac{a_i}{16\pi^2}g_i^3 + \frac{1}{(16\pi^2)^2}\sum_j b_{ij}g_i^3 g_j^2, \tag{75}$$

where $a_i(b_{ij})$ are one-loop (two-loop) beta function coefficients. Their values for the Model I and Model II are given in Table 5.

11 Appendix B

11.1 Block diagonalisation and determination of $\mathcal{M}_\nu$

In this section we discuss the various steps of block diagonalisation in order to calculate the light-neutrino mass, sterile neutrino mass and right-handed neutrino mass and their mixings. The complete 9×9 mass matrix in the flavour basis $\{\nu_L, S_L, N_R^C\}$ is

Table 5 One-loop and two-loop beta function coefficients for gauge coupling evolutions described in the text taking the second Higgs doublet mass at 1 TeV

Symmetry	a_i	b_{ij}
G_{213}	$(-19/6, 41/10, -7)$	$\begin{pmatrix} 199/50, 27/10, 44/5 \\ 9/10, 35/6, 12 \\ 11/10, 9/2, -26 \end{pmatrix}$
G_{2113}	$(-3, 57/12, 37/8, -7)$	$\begin{pmatrix} 8, 1, 3/2, 12 \\ 3/2, 33/57, 63/8, 12 \\ 9/2, 63/8, 209/16, 4 \\ 9/2, 3/2, 1/2, 26 \end{pmatrix}$
G_{2213}	$(-2, -3/2, 29/4, -7)$	$\begin{pmatrix} 31, 6, 39/2, 12 \\ 6, 115/6, 3/2, 12 \\ 81/2, 6, 181/8, 4 \\ 9/2, 9/2, 1/2, -26 \end{pmatrix}$
G_{2213D}	$(-3/2, -3/2, 15/2, -7)$	$\begin{pmatrix} 319/6, 6, 57/4, 12 \\ 6, 319/6, 57/4, 12 \\ 171/4, 171/4, 239/4, 4 \\ 9/2, 9/2, 1/2, -26 \end{pmatrix}$

$$\mathcal{M} = \begin{pmatrix} m_\nu^{II} & M_L & M_D \\ M_L^T & 0 & M \\ M_D^T & M^T & M_N \end{pmatrix}, \tag{76}$$

where $M_L = y_\chi v_{\chi L}$, $M = y_\chi v_{\chi R}$, $M_N = f v_R$ and M_D is the Dirac neutrino mass matrix as discussed in Sect. 4.

Assuming a generalised unitary transformation from mass basis to flavour basis gives

$$|\psi\rangle_{\text{flavour}} = \mathcal{V}\,|\psi\rangle_{\text{mass}} \tag{77}$$

or

$$\begin{pmatrix} \nu_\alpha \\ S_\beta \\ N_\gamma^C \end{pmatrix} = \begin{pmatrix} \mathcal{V}_{\alpha i}^{\nu\nu} & \mathcal{V}_{\alpha j}^{\nu S} & \mathcal{V}_{\alpha k}^{\nu N} \\ \mathcal{V}_{\beta i}^{S\nu} & \mathcal{V}_{\beta j}^{SS} & \mathcal{V}_{\beta k}^{SN} \\ \mathcal{V}_{\gamma i}^{N\nu} & \mathcal{V}_{\gamma j}^{NS} & \mathcal{V}_{\gamma k}^{NN} \end{pmatrix} \begin{pmatrix} \hat{\nu}_i \\ \hat{S}_j \\ \hat{N}_k \end{pmatrix} \tag{78}$$

with

$$\mathcal{V}^\dagger \mathcal{M} \mathcal{V}^* = \hat{\mathcal{M}} = \text{diag}\left(\hat{\mathcal{M}}_{\nu_i}; \hat{\mathcal{M}}_{\mathcal{S}_j}; \hat{\mathcal{M}}_{\mathcal{N}_k}\right). \tag{79}$$

Here $\mathcal{M}_\nu$ is the 9×9 neutral fermion mass matrix in a flavour basis with α, β, γ running over three generations of light-neutrinos, sterile-neutrinos and right handed heavy-neutrinos in their respective flavour states and $\hat{\mathcal{M}}_\nu$ is the diagonal mass matrix with $(i, j, k = 1, 2, 3)$ running over corresponding mass states.

In the first step of block diagonalisation, the full neutrino mass matrix is reduced to a block-diagonal form $\hat{\mathcal{M}}_{\text{BD}}$ and in the second step we further block diagonalise to obtain the three matrices as three different block-diagonal elements, $\mathcal{M}_{\text{BD}} = \text{diag}(\mathcal{M}_\nu, m_S, m_N)$ whose each diagonal element is a 3×3 matrix. In our estimation, we have used the mass hierarchy $M_N > M \gg M_D, M_L, f v_L$. Finally in the third

step we discuss a complete diagonalisation to arrive at the physical masses and their mixings.

11.2 Determination of $\mathcal{M}_{\rm BD}$

With the two unitary matrix transformations $\mathcal{Q}_1$ and $\mathcal{Q}_2$,

$$\mathcal{Q}^\dagger \mathcal{M}_\nu \mathcal{Q}^* = \hat{\mathcal{M}}_{\rm BD}, \tag{80}$$

where

$$\mathcal{Q} = \mathcal{Q}_1\, \mathcal{Q}_2, \tag{81}$$

i.e. the product matrix $\mathcal{Q} = \mathcal{Q}_1\, \mathcal{Q}_2$ directly give $\mathcal{M}_{\rm BD}$ from $\mathcal{M}_\nu$ Here $\hat{\mathcal{M}}_{\rm BD}$ and $\mathcal{M}_{\rm BD}$ are the intermediate block-diagonal and full block-diagonal mass matrices, respectively,

$$\hat{\mathcal{M}}_{\rm BD} = \begin{pmatrix} \mathcal{M}_{\rm eff} & 0 \\ 0 & m_N \end{pmatrix} \tag{82}$$

and

$$\mathcal{M}_{\rm BD} = \begin{pmatrix} \mathcal{M}_\nu & 0 & 0 \\ 0 & m_S & 0 \\ 0 & 0 & m_N \end{pmatrix}. \tag{83}$$

11.3 Determination of $\mathcal{Q}_1$

In the leading order parametrisation the standard form of $\mathcal{Q}_1$ is

$$\mathcal{Q}_1 = \begin{pmatrix} 1 - \frac{1}{2} R^* R^T & R^* \\ -R^T & 1 - \frac{1}{2} R^T R^* \end{pmatrix}, \tag{84}$$

where R is a 6×3 dimensional matrix. We have

$$R^\dagger = M_N^{-1} \left(M_D^T, M^T \right) = (K^T, J^T) \tag{85}$$

$$J = M M_N{}^{-1} K = M_D M_N^{-1} I = K J^{-1} = M_D M^{-1}. \tag{86}$$

Therefore, the transformation matrix $\mathcal{Q}_1$ can be written purely in terms of the dimensionless parameters J and K,

$$\mathcal{Q}_1 = \begin{pmatrix} 1 - \frac{1}{2} K K^\dagger & -\frac{1}{2} K J^\dagger & K \\ -\frac{1}{2} J K^\dagger & 1 - \frac{1}{2} J J^\dagger & J \\ -K^\dagger & -J^\dagger & 1 - \frac{1}{2}(K^\dagger K + J^\dagger J) \end{pmatrix}, \tag{87}$$

while the light and heavy mass matrices are

$$\mathcal{M}_{\rm eff} = \begin{pmatrix} f v_L & M_L \\ M_L^T & 0 \end{pmatrix} - \begin{pmatrix} M_D M_N^{-1} M_D^T & M_D M_N^{-1} M \\ M^T M_N^{-1} M_D^T & M^T M_N^{-1} M \end{pmatrix}, \tag{88}$$

$$m_N = M_N + \cdots. \tag{89}$$

We denote

$$\mathcal{M}_{\rm eff} = \begin{pmatrix} Z & B \\ C & D \end{pmatrix}, \tag{90}$$

$$Z = f v_L - M_D M_N^{-1} M_D^T, \tag{91}$$

$$B = M_L - M_D M_N^{-1} M, \tag{92}$$

$$C = M_L^T - M^T M_N^{-1} M_D^T, \tag{93}$$

$$D = M^T M_N^{-1} M. \tag{94}$$

11.4 Determination of $\mathcal{Q}_2$

The remaining mass matrix $\mathcal{M}_{\rm eff}$ can be further block diagonalised using another transformation matrix,

$$\mathcal{S}^\dagger \mathcal{M}_{\rm eff} \mathcal{S}^* = \begin{pmatrix} \mathcal{M}_\nu & 0 \\ 0 & m_S \end{pmatrix} \tag{95}$$

such that in Eq. (11.2)

$$\mathcal{Q}_2 = \begin{pmatrix} \mathcal{S} & 0 \\ 0 & 1 \end{pmatrix}, \tag{96}$$

$$S = \begin{pmatrix} 1 - \frac{1}{2} P^* P^T & P^* \\ -P^T & 1 - \frac{1}{2} P^T P^* \end{pmatrix}. \tag{97}$$

Using Eq. (97) in Eq. (95), we get through Eqs. (90)–(94)

$$\begin{aligned} P^\dagger &= (M^T M_N^{-1} M)^{-1} \left(M^T M_N^{-1} M_D^T - M_L^T \right) \\ &= M^{-1} M_D^T - M^{-1} M_N M^{-1} M_L \end{aligned} \tag{98}$$

where we have used that y_χ is symmetric, leading to

$$\begin{aligned} \mathcal{M}_\nu = m_\nu^{II} &+ \left(M_D M_N^{-1} M_D^T \right) \\ &- (M_D M_N^{-1} M_D^T) + M_L (M^T M_N^{-1} M)^{-1} M_L^T \\ &- M_L (M^T M_N^{-1} M)^{-1} (M^T M_N^{-1} M_D^T) \\ &- (M_D M_N^{-1} M)(M^T M_N^{-1} M)^{-1} M_L^T, \\ m_S = &- M M_N^{-1} M^T + \cdots. \end{aligned} \tag{99}$$

The 3×3 block-diagonal mixing matrix $\mathcal{Q}_2$ has the following form:

$$\mathcal{Q}_2 = \begin{pmatrix} S & \mathbf{0} \\ \mathbf{0} & \mathbf{1} \end{pmatrix} = \begin{pmatrix} 1 - \frac{1}{2} I I^\dagger & I & 0 \\ -I^\dagger & 1 - \frac{1}{2} I^\dagger I & 0 \\ 0 & 0 & 1 \end{pmatrix} \tag{100}$$

where we have used Eq. (86) to define $I = K J^{-1} = M_D M^{-1}$.

Complete diagonalisation and physical neutrino masses The 3×3 block-diagonal matrices $\mathcal{M}_\nu, m_S$ and m_N can further be diagonalised to give physical masses for all neutral leptons by a 9×9 unitary matrix $\mathcal{U}$ as

$$\mathcal{U} = \begin{pmatrix} U_\nu & 0 & 0 \\ 0 & U_S & 0 \\ 0 & 0 & U_N \end{pmatrix}, \tag{101}$$

where the 3×3 unitary matrices U_ν, U_S and U_N satisfy

$$U_\nu^\dagger \, \mathcal{M}_\nu \, U_\nu^* = \hat{\mathcal{M}}_\nu = \text{diag}\,(\mathcal{M}_{\nu 1}, \mathcal{M}_{\nu 2}, \mathcal{M}_{\nu 3})\,,$$
$$U_S^\dagger \, m_S \, U_S^* = \hat{m_S} = \text{diag}\,(m_{S1}, m_{S2}, m_{S3})\,,$$
$$U_N^\dagger \, m_N \, U_N^* = \hat{m_N} = \text{diag}\,(m_{N1}, m_{N2}, m_{N3})\,. \qquad (102)$$

With this discussion, the complete mixing matrix is

$$\begin{aligned}
\mathcal{V} &= \mathcal{Q} \cdot \mathcal{U} = (\mathcal{Q}_1 \cdot \mathcal{Q}_2 \cdot \mathcal{U}) \\
&= \begin{pmatrix} 1 - \frac{1}{2} K K^\dagger & -\frac{1}{2} K J^\dagger & K \\ -\frac{1}{2} J K^\dagger & 1 - \frac{1}{2} J J^\dagger & J \\ -K^\dagger & -J^\dagger & 1 - \frac{1}{2}(K^\dagger K + J^\dagger J) \end{pmatrix} \cdot \\
&\begin{pmatrix} 1 - \frac{1}{2} I I^\dagger & I & 0 \\ -I^\dagger & 1 - \frac{1}{2} I^\dagger I & 0 \\ 0 & 0 & 1 \end{pmatrix} \begin{pmatrix} U_\nu & 0 & 0 \\ 0 & U_S & 0 \\ 0 & 0 & U_N \end{pmatrix} \\
&= \begin{pmatrix} 1 - \frac{1}{2} I I^\dagger & I - \frac{1}{2} K J^\dagger & K \\ -I^\dagger & 1 - \frac{1}{2}(I^\dagger I + J J^\dagger) & J - \frac{1}{2} I^\dagger K \\ 0 & -J^\dagger & 1 - \frac{1}{2} J^\dagger J \end{pmatrix} \cdot \begin{pmatrix} U_\nu & 0 & 0 \\ 0 & U_S & 0 \\ 0 & 0 & U_N \end{pmatrix}. \qquad (103)
\end{aligned}$$

References

1. H.V. Klapdor-Kleingrothaus, A. Dietz, L. Baudis, G. Heusser, I.V. Krivosheina, S. Kolb, B. Majorovits, H. Pas, H. Strecker, V. Alexeev, A. Balysh, A. Bakalyarov, S.T. Belyaev, V.I. Lebedev, S. Zhukov, Kurchatov Institute, Moscow, Russia. Eur. Phys. J. A **12**, 147 (2001)
2. C. Arnaboldi et al., CUORICINO Collaboration. Phys. Rev. C **78**, 035502 (2008)
3. C.E. Aalseth et al., IGEX Collaboration. Phys. Rev. D **65**, 092007 (2002)
4. J. Argyriades et al., NEMO Collaboration. Phys. Rev. C **80**, 032501 (2009)
5. I. Abt, M.F. Altmann, A. Bakalyarov, I. Barabanov, C. Bauer, E. Bellotti, S.T. Belyaev, L.B. Bezrukov et al. [hep-ex/0404039]
6. S. Schonert et al., GERDA Collaboration. Nucl. Phys. Proc. Suppl. **145**, 242 (2005)
7. C. Arnaboldi et al., CUORE Collaboration. Nucl. Instrum. Meth. A **518**, 775 (2004)
8. H.V. Klapdor-Kleingrothaus, I.V. Krivosheina, A. Dietz, O. Chkvorets, Phys. Lett. B **586**, 198 (2004)
9. H.V. Klapdor-Kleingrothaus, I.V. Krivosheina, Mod. Phys. Lett. A **21**, 1547 (2006)
10. J.C. Pati, A. Salam, Phys. Rev. D **8**, 1240 (1973)
11. J.C. Pati, A. Salam, Phys. Rev. D **10**, 275 (1974)
12. R.N. Mohapatra, J.C. Pati, Phys. Rev. D **11**(566), 2558 (1975)
13. G. Senjanović, R.N. Mohapatra, Phys. Rev. D **12**, 1502 (1975)
14. K.S. Babu, R.N. Mohapatra, Phys. Rev. Lett. **70**, 2845 (1993)
15. M. Kadastik, K. Kanike, M. Raidal, Phys. Rev. D **80**, 085020 (2009)
16. M. Frigerio, T. Hambye, Phys Rev. D **81**, 075002 (2010)
17. M.K. Parida, P.K. Sahu, K. Bora, Phys. Rev. D **83**, 093004 (2011)
18. M.K. Parida, Phys. Lett. B **704**, 206 (2011)
19. M.K. Parida, Pramana **79**, 1271 (2012)
20. P. Minkowski, Phys. Lett. B **67**, 421 (1977)
21. T. Yanagida in Workshop on Unified Theories, KEK Report 79–18, p. 95, 1979
22. M. Gell-Mann, P. Ramond, R. Slansky, *Supergravity* (North Holland, Amsterdam, 1979), p. 315
23. S.L. Glashow, *1979 Cargese Summer Institute on Quarks and Leptons* (Plenum, New York, 1980), p. 687
24. R.N. Mohapatra, G. Senjanovic, Phys. Rev. Lett. **44**, 912 (1980)
25. J.J. Schechter, J.W.F. Valle, Phys. Rev. D **22**, 2227 (1980)
26. J.J. Schechter, J.W.F. Valle, Phys. Rev. D **25**, 774 (1982)
27. D. Aristizabal Sierra, M. Tortola, J.W.F. Valle, A.Vicente. arXiv:1405.4706V2 [hep-ph]
28. Y. Fukuda et al., SuperKamiokande Collaboration. Phys. Rev. Lett. **81**, 1562–1567 (1998)
29. J. Schechter, J.W.F. Valle, Phys. Rev. D **22**, 2227 (1980)
30. M. Magg, C. Wetterich, Phys. Lett. B **94**, 61 (1980)
31. G. Lazaridis, Q. Shafi, C. Wetterich, Nucl. Phys. B **181**, 287 (1981)
32. P.S. Bhupal Dev, R.N. Mohapatra. Phys. Rev. D **81**, 013001 (2010)
33. M. K. Parida, A. Raychaudhuri. Phys. Rev. D **26**, 2364 (1982)
34. M.K. Parida, C.C. Hazra, Phys. Lett. B **121**, 355 (1983)
35. M.K. Parida, C.C. Hazra, Phys. Rev. D **40**, 3074 (1989)
36. R.L. Awasthi, M.K. Parida, Phys. Rev. D **86**, 093004 (2012)
37. R.L. Awasthi, M.K. Parida, S. Patra, J. High Energy Phys. **1308**, 122 (2013). arXiv:1302.0672 [hep-ph]
38. P. Athanasopoulos, A.E. Faraggi, V.M. Mehta, Phys. Rev. D **89**, 105023 (2014)
39. M.K. Parida, R.L. Awasthi, P.K. Sahu. arXiv:1401.1412 [hep-ph]
40. R.N. Mohapatra, M.K. Parida, G. Rajasekaran, Phys. Rev. D **72**, 013002 (2004)
41. R.N. Mohapatra, M.K. Parida, G. Rajasekaran, Phys. Rev. D **72**, 013002 (2005)
42. R.N. Mohapatra, M.K. Parida, G. Rajasekaran, Phys. Rev. D **71**, 057301 (2005)
43. S.K. Agarwalla, M.K. Parida, R.N. Mohapatra, G. Rajasekaran, Phys. Rev. D **75**, 033007 (2007)
44. B. Bajc, G. Senjanovic, F. Vissani, Phys. Rev. Lett. **90**, 051802 (2003)
45. H.S. Goh, R.N. Mohapatra, S.P. Ng, Phys. Rev. D **68**, 11508 (2003)
46. K.S. Babu, C. Macesanu, Phys. Rev. D **72**, 115003 (2005)
47. B. Dutta, Y. Mimura, R.N. Mohapatra, Phys. Rev. D **69**, 115014 (2004)
48. S. Bertollini, M. Frigerio, M. Malinsky, Phys. Rev. D **70**, 095002 (2004)
49. S. Bertollini, T. Schwetz, M. Malinsky, Phys. Rev. D **73**, 115012 (2006)
50. C.S. Aulakh, S.K. Garg. arXiv:0807.0917 [hep-ph]
51. B. Dutta, Y. Minura, R.N. Mohapatra, Phys. Rev. D **80**, 095021 (2009)
52. A. Joshipura, B.P. Kodrani, K.M. Patel, Phys. Rev. D **79**, 115017 (2009)
53. G. Altarelli, G. Blankenburg, J. High Energy Phys. **1103**, 133 (2011)
54. P.S. Bhupal Dev, R.N. Mohapatra, M. Severson, Phys. Rev. D **84**, 053005 (2011)
55. P.S. Bhupal Dev, B. Dutta, R.N. Mohapatra, M. Severson. arXiv:1202.4012 [hep-ph]
56. R.N. Mohapatra, M.K. Parida, Phys. Rev. D **84**, 095021 (2011)
57. H.S. Goh, R.N. Mohapatra, S. Nasri, Phys. Rev. D **70**, 075022 (2004)
58. R.N. Mohapatra, G. Senjanovic, Phys. Rev. D **23**, 165 (1981)
59. D. Chang, R.N. Mohapatra, M.K. Parida, Phys. Rev. Lett. **52**, 1072 (1984)
60. D. Chang, R.N. Mohapatra, M.K. Parida, Phys. Rev. D **30**, 1052 (1984)
61. D. Chang, R.N. Mohapatra, Phys. Rev. D **32**, 1248 (1985)
62. D. Chang, R.N. Mohapatra, J. Gipson, R.E. Marshak, M.K. Parida, Phys. Rev. D **31**, 1718 (1985)
63. M.K. Parida, Phys. Lett. B **126**, 220 (1983)
64. M.K. Parida, Phys. Rev. D **17**, R2383 (1983)
65. M.K. Parida, A. Raychaudhuri, Phys. Rev. D **82**, 093017 (2010)
66. P. Langacker, Rev. Mod. Phys. **81**, 1199 (2009)

67. P. Langacker, R.W. Robinet, J.L. Rosner, Phys. Rev. D **30**, 1470 (1984)
68. P. Langacker, Phys. Rev. D **30**, 2008 (1984)
69. K.S. Babu et al. arXiv:1311.5285 [hep-ex]
70. A. de Gouvea et al. arXiv:1310.4340 [hep-ex]
71. K. Abe et al. arXiv:1305.4391 [hep-ex]
72. K. Abe et al. arXiv:1307.0162 [hep-ex]
73. P. Nath, P.F. Perez, Phys. Rept. (2007)
74. B. Bajc, I. Dorsner, M. Nemevsek, J. High Energy Phys. **0811**, 007 (2008)
75. P. Langacker, Phys. Rept. **72**, 185 (1981)
76. R.N. Mohapatra, Phys. Rev. Lett. **56**, 61 (1986)
77. R.N. Mohapatra, J.W.F. Valle, Phys. Rev D **34**, 1642 (1986)
78. M.K. Parida, Sudhanwa Patra. Phys. Lett. B **718**, 1407 (2013)
79. W. Grimus, L. Lavoura, JHEP **0011**, 042 (2000). arXiv:hep-ph/0008179
80. M. Mitra, G. Senjanovic, F. Vissani, Nucl. Phys. B **856**, 26 (2012)
81. M. Hirsch, H.V. Klapdor-Kleingrothaus, O. Panella, Phys. Lett. B **374**, 7 (1996). arXiv:hep-ph/9602306
82. S. Pascoli, M. Mitra, Steven Wong. arXiv:1310.6218 [hep-ph]
83. M. Lindner, M.A. Schmidt, A. Yu Smirnov, J. High Energy Phys. **0507**, 048 (2005)
84. S.M. Barr, Phys. Rev. Lett. **92**, 101601 (2004)
85. S.M. Barr, B. Kyae, Phys. Rev. D **71**, 075005 (2004)
86. F. Deppisch, T.S. Kosmas, J.W.F. Valle, Nucl. Phys. B **752**, 80 (2006)
87. J. Garoya, M.C. Gonjalez-Gartia, N. Rius, J. High Energy Phys. **02**, 021 (2007)
88. C. Arina, F. Bazzochi, N. Forengo, J.C. Romao, J.W.F. Valle, Phys. Rev. Lett. **101**, 161802 (2008)
89. M.B. Gavela, T. Hambye, D. Hernandez, P. Hernandez, J. High Energy Phys. **09**, 038 (2009)
90. M. Malinsky, T. Ohlsson, Z.-z. Xing, H. Zhang, Phys. Lett. B **679**, 242 (2009)
91. M. Hirsch, T. Kernreiter, J.C. Romao, A. Villanova del Moral, J. High Energy Phys. **1001**, 103 (2010). arXiv:0910.2435 [hep-ph]
92. M.B. Gavela, T. Hambye, D. Hernandez, P. Hernandez, J. High Energy Phys. **09**, 038 (2009)
93. A. Das, N. Okada, Phys. Rev. D **88**, 103001 (2013)
94. P.S. BhupalDev, A. Pilaftsis. arXiv:1209.4051 [hep-ph]
95. A. Das, P.S. Bhupal, Dev, N. Okada. Phys. Lett. B **735**, 364 (2014)
96. G. 't Hooft, in *Proceedings of the 1979 Cargese Summer Institute on Recent Developments in Gauge Theories*, ed. by G. 't Hooft et al. (Plenum Press, New York, 1980)
97. S.K. Kang, C.S. Kim, Phys. Lett. B **646**, 248 (2007)
98. J. Ellis, D.V. Nanopoulos, K. Olive, Phys. Lett. B **300**, 121 (1993)
99. S.K. Majee, M.K. Parida, A. Raychaudhuri, Phys. Lett. **668**, 299 (2008)
100. M.K. Parida, A. Raychaudhuri, Phys. Rev. D **82**, 093017 (2010)
101. S.K. Majee, M.K. Parida, A. Raychaudhuri, U. Sarkar, Phys. Rev. D **75**, 075003 (2007)
102. G.L. Fogli, E. Lisi, A. Marrone, A. Palazzo, A.M. Rotuno, Nucl. Phys. B. Proc. Suppl. **188**, 27 (2009)
103. T. Schwetz, M. Tartola, J.W.F. Valle, New J. Phys. **13**, 063004 (2011)
104. D.V. Forero, M. Tartola, J.W.F. Valle. arXiv:1205.4018 [hep-ph]
105. K. Abe et al., [T2K collaboration], Phys. Rev. Lett. **107**, 041801 (2011). arXiv:1106.2822
106. C.R. Das, M.K. Parida, Eur. Phy. J. C **20**, 121 (2001)
107. M.K. Parida, B. Purkayastha, Eur. Phy. J C **14**, 159 (2000)
108. M.K. Parida, N.N. Singh, Phys. Rev. D **59**, 32022 (1999)
109. F.M. Almeida Jr, Y.A. Countinho, J.A. Martins Simoes, M. A.B. do Vale, Phys. Rev. D **62**, 075004 (2000). arXiv:hep-ph/0002024
110. S. Antusch, J.P. Baumann, E. Fernandez-Martinez, Nucl. Phys. B **180**, 369 (2009)
111. S. Antusch, J.P. Baumann, E. Fernandez-Martinez, J. Lopez-Pavon, Nucl. Phys. B **810**, 369 (2009)
112. S. Antush, C. Biggio, E. Fernandez-Martinez, M. Belen Gavela, J. Lopez-Pavon, J. High Energy Phys. **10**, 084 (2006)
113. D.V. Forero, S. Morisi, M. Tartola, J.W.F. Valle, J. High Energy Phys. **09**, 142 (2011)
114. A. Ilakovac, A. Pilaftsis, Nucl. Phys. B **437**, 491 (1995). [hep-ph/9403398]
115. F. Deppisch, J.W.F. Valle, Phys. Rev. D **72**, 036001 (2005). [hep-ph/0406040]
116. C. Arina, F. Bazzocchi, N. Fornengo, J.C. Romao, J.W.F. Valle, Phys. Rev. Lett. **101**, 161802 (2008). arXiv:0806.3225 [hep-ph]
117. M. Malinsky, T. Ohlsson, Z. Xing, H. Zhang, Phys. Lett. B **679**, 242–248 (2009). arXiv:0905.2889 [hep-ph]
118. M. Hirsch, T. Kernreiter, J.C. Romao, A. Villanova del Moral, JHEP **1001**, 103 (2010). arXiv:0910.2435 [hep-ph]
119. F. Deppisch, T.S. Kosmas, J.W.F. Valle, Nucl. Phys. B **752**, 80 (2006). arXiv:0910.3924 [hep-ph]
120. S.P. Das, F.F. Deppisch, O. Kittel, J.W.F. Valle, Phys. Rev. D **86**, 055006 (2012)
121. J. Adam et al. (MEG Collaboration), Phys. Rev. Lett. **107**, 171801 (2011). arXiv:1107.5547 [hep-ex]
122. K. Hayasaka et al., (Belle Collaboration), Phys. Lett. B **666**, 16 (2008). arXiv:0705.0650 [hep-ex]
123. M.L. Brooks et al., MEG Collaboration. Phys. Rev. Lett. **83**, 1521 (1999)
124. B. Aubert [The BABAR Collaboration]. arXiv:0908.2381 [hep-ex]
125. Y. Kuno (PRIME Working Group), Nucl. Phys. B. Proc. Suppl. **149**, 376 (2005)
126. For a review see F.R. Joaquim, A. Rossi, Nucl. Phys. B **765**, 71 (2007)
127. E. Fernandez-Martinez, M.B. Gavela, J. Lopez-Pavon, O. Yasuda, Phys. Lett. B **649**, 427 (2007)
128. K. Kanaya, Prog. Theor. Phys. **64**, 2278 (1980)
129. J. Kersten, A.Y. Smirnov, Phys. Rev. D **76**, 073005 (2007)
130. M. Malinsky, T. Ohlsson, H. Zhang, Phys. Rev. D **79**, 073009 (2009)
131. G. Altarelli, D. Meloni, Nucl. Phys. B **809**, 158 (2009)
132. F. del Aguila, J.A. Aguilar-Saavedra, Phys. Lett. B **672**, 158 (2009)
133. F. del Aguila, J.A. Aguilar-Saavedra, J. de Blas, Acta Phys. Polon. B **40**, 2901 (2009). arXiv:0910.2720 [hep-ph]
134. A. van der Schaaf, J. Phys. G **29**, 2755 (2003)
135. Y. Kuno, Nucl. Phys. B, Proc. Suppl. **149**, 376 (2005)
136. R.N. Mohapatra, Phys. Rev. D **34**, 909 (1986)
137. M. Doi, T. Kotani, Prog. Theor. Phys. **89**, 139 (1993)
138. K. Muto, I. Blender, H.V. Klapdor-Kleingrothaus, Z. Phys A **334**, 177 (1989)
139. M. Hirsch, K. Muto, T. Oda, H.V. Klapdor-Kleingrothaus, Z. Phys A **347**, 151 (1994)
140. J.J. Gomez-Cadenas, J. Martin-Albo, M. Mezzetto, F. Monrabal, M. Sorel, Riv. Nuovo Cim. **35**, 29 (2012). arXiv:1109.5515 [hep-ex]
141. J. Lopez-Pavon, S. Pascoli, C.-f. Wong. arXiv:1209.5342
142. J. Suhonen, O. Civitarese, Phys. Rept. C **300**, 123 (1998)
143. J. Kotila, F. Iachello, Phys. Rev. C **85**, 034316 (2012). arXiv:1209.5722 [nucl-th]
144. M. Doi, T. Kotani, E. Takasugi, Prog. Theor. Phys. Suppl. **83**, 1 (1985)
145. F. Simkovic, G. Pantis, J. Vergados, A. Faessler, Phys. Rev. C **60**, 055502 (1999). arXiv:hep-ph/9905509 [hep-ph]
146. A. Faessler, A. Meroni, S.T. Petcov, F. Simkovic, J. Vergados, Phys. Rev. D **83**, 113003 (2011). arXiv:1103.2434 [hep-ph]
147. G. Pantis, F. Simkovic, J. Vergados, A. Faessler, Phys. Rev. C **53**, 695 (1996). arXiv:nucl-th/9612036 [nucl-th]

148. A. Pilaftsis, T.E.J. Underwood, Nucl. Phys. B **692**, 303 (2004). arXiv:hep-ph/0309342
149. M.K. Parida, Bidyut Prava Nayak (Work in progress)
150. M. Ciuchini, E. Franco, S. Mishima, L. Silvestrini. arXiv:1306.4644 [hep-ph]
151. M.E. Peskin, T. Takeuchi, Phys. Rev. Lett. **65**, 964 (1990)
152. M.E. Peskin, T. Takeuchi, Phys. Rev. D **46**, 381 (1992)
153. T. Appelquist, B.A. Dobrescu, A.R. Hopper, Phys. Rev. D **68**, 035012 (2003). arXiv:hep-ph/0212073
154. F. Jegerlehner, M. YU. Kalmykov, B. Kniehl, Phys. Lett. B **722**, 123 (2013). arXiv:1212.4319 [hep-ph]
155. J. Erler, P. Langacker, S. Munir, E. Roja, JHEP **08**, 017 (2009). arXiv:0906.2435 [hep-ph]
156. J. Erler, P. Langacker. arXiv:1108.0685 [hep-ph]
157. T. Han, P. Langacker, Z. Liu, L.-T. Wang. arXiv:1308.2738 [hep-ph]
158. CMS Collaboration, CMS-PAS-HIG-13-005
159. ATLAS Collaboration, ATLAS-CONF-2013-014
160. ATLAS-COM-CONF-2013-025
161. K.A. Olive et al., Particle Data Group. Chin. Phys. C **38**, 090001 (2014)
162. K. Nakamura et al., Particle Data Group. J. Phys. G **37**, 075021 (2010)
163. C. Amsler et al., Particle Data Group. Phys. Lett. B **667**, 1 (2008)
164. J.C. Montero, V. Pleitez, Phys. Lett. B **765**, 64 (2009). arXiv:0706.0473 [hep-ph]
165. E.C.F.S. Fortes, J.C. Montero, V. Pleitez, Phys. Rev. D **82**, 114007 (2010). arXiv:1005.2991 [hep-ph]
166. V.V. Andreev, G.M. Pick, P. Osland, Eur. Phys. J. C **72**, 2147 (2012)
167. T. Hambye, G. Senjanovic, Phys. Lett. B **582**, 73 (2004)
168. S. Blanchet, T. Hambye, F.X. Josse-Michaux, JHEP **1004**, 023 (2010)
169. Y. Ahn, S.K. Kang, C.S, Kim, T.P. Nguyen. Phys. Rev. D **82**, 093005 (2010)
170. A. Pilaftsis, Phys. Rev. D **56**, 5431 (1997)